About Fourier optics

Éric Thiébaut

October 15, 2024

These notes are my attempt to collect the equations for numerical modeling of optical systems by physical optics propagation (POP). I tried to provide consistent results with a unified and readable notation[1], with simple demonstrations not forgetting the hypotheses that must hold and the assumed conventions.

Contents

1 Theory of scalar waves propagation **2**
- 1.1 From Maxwell equations to Helmholtz equation . . . 2
- 1.2 Elementary solutions to the Helmholtz equation . . . 3
  - 1.2.1 Plane wave . . . 3
  - 1.2.2 Spherical wave . . . 4
- 1.3 The Helmholtz equation for the modulation of a carrier wave . . . 5
- 1.4 Diffraction by a surface . . . 6
- 1.5 Diffraction by a planar surface . . . 7
  - 1.5.1 Planar diffraction seen as a convolution . . . 7
  - 1.5.2 The angular spectrum solution . . . 8
  - 1.5.3 Interpretation of the angular spectrum . . . 11
  - 1.5.4 Rayleigh-Sommerfeld diffraction . . . 12
- 1.6 Paraxial approximation: Fresnel diffraction . . . 13
  - 1.6.1 The angular spectrum transfer function at low frequencies . . . 13
  - 1.6.2 Modulation of a plane carrier wave . . . 15
  - 1.6.3 From Rayleigh-Sommerfeld diffraction to Fresnel diffraction . . . 16
  - 1.6.4 Alternative formulation of Fresnel diffraction integral . . . 17
  - 1.6.5 Planar wave in the paraxial approximation. . . . 18
  - 1.6.6 Spherical wave in the paraxial approximation. . . . 18
  - 1.6.7 Propagation of Gaussian beams in the paraxial approximation 18
- 1.7 Fraunhofer diffraction . . . 18

[1] of course this is highly subjective

2 Propagation methods **19**
2.1 Sampling . . . 20
2.2 Propagation by convolution . . . 23
2.2.1 Support constraint in propagation by convolution . . . 24
2.2.2 Sampling and range constraints in Rayleigh-Sommerfeld diffraction . . . 26
2.2.3 Sampling and range constraints for paraxial propagation kernel 28
2.3 Angular spectrum propagation . . . 29
2.4 Angular spectrum frequencies . . . 30
2.4.1 Propagation by the non-paraxial transfer function . . . 31
2.4.2 Propagation by the paraxial transfer function . . . 32
2.5 Propagation by the Fresnel transform . . . 33
2.6 Discrete computations . . . 33

3 Optical components **40**
3.1 Point source . . . 40
3.2 Thin lens . . . 40

A The field as a superposition of plane waves **41**

B Tilted paraxial approximation **43**

C The discrete Fourier transform **46**
C.1 Uni-dimensional case . . . 46
C.2 Multi-dimensional case . . . 48

1 Theory of scalar waves propagation

1.1 From Maxwell equations to Helmholtz equation

This part is based on the book of Goodman (1996). In a medium with **no free charges**, Maxwell equations yield:

$$\nabla^2 \boldsymbol{U} + 2\,\nabla(\boldsymbol{U} \cdot \nabla \log n) = \frac{n^2}{c^2}\,\frac{\partial^2 \boldsymbol{U}}{\partial t^2}. \tag{1}$$

where $\boldsymbol{U} \in \mathbb{R}^3$ is either the electric field or the magnetic field as a function of space and time, n is the refractive index of the medium, c is the light speed in vacuum, t is the time, ∇ denotes spatial derivative, and ∇^2 is the Laplacian operator.

In an **homogeneous medium**, $\nabla \log n = 0$ and Eq. (1) simplifies to:

$$\nabla^2 \boldsymbol{U} = \frac{n^2}{c^2}\,\frac{\partial^2 \boldsymbol{U}}{\partial t^2} \tag{2}$$

which holds separately for the Cartesian components of $\boldsymbol{U}$ because the Laplacian of the vector field $\boldsymbol{U}$ writes:

$$\nabla^2 \boldsymbol{U} = (\nabla^2 U_x)\,\boldsymbol{e}_x + (\nabla^2 U_y)\,\boldsymbol{e}_y + (\nabla^2 U_z)\,\boldsymbol{e}_z \tag{3}$$

where (U_x, U_y, U_z) are the Cartesian components of $\boldsymbol{U}$ while $\boldsymbol{e}_x$, $\boldsymbol{e}_y$, and $\boldsymbol{e}_z$ are unit vectors along the corresponding Cartesian axes. Hence, the propagation equation simply writes:

$$\nabla^2 U(\boldsymbol{r}, t) = \frac{n^2}{c^2} \frac{\partial^2 U(\boldsymbol{r}, t)}{\partial t^2} \tag{4}$$

for any Cartesian component $U(\boldsymbol{r}, t) = U_x$, U_y, or U_z of $\boldsymbol{U}$. In the **scalar field theory**, the propagation of the field $\boldsymbol{U}$ is reduced to that of the component $U(\boldsymbol{r}, t)$. Working with $U(\boldsymbol{r}, t)$ is much simpler but is an approximation. In an inhomogeneous medium, the term $\nabla\big(\boldsymbol{U} \cdot \nabla \log n\big)$ introduces some coupling between the components of the field $\boldsymbol{U}$. Even though the medium is homogeneous, at close distances (a few wavelengths) of the edges of diffracting material, the coupling between the electric and magnetic fields and between their components is not negligible.

For a **monochromatic** electromagnetic wave, the scalar field is a separable function of the position $\boldsymbol{r}$ and of the time t which can be expressed as:

$$\boxed{U(\boldsymbol{r}, t) = \mathrm{Re}\Big(u(\boldsymbol{r})\, \mathrm{e}^{-\mathrm{i}\, 2\, \pi\, \nu\, t}\Big)} \tag{5}$$

with $\nu > 0$ the temporal frequency and where $u(\boldsymbol{r}) \in \mathbb{C}$ is a scalar field, called the **complex amplitude**, that only depends on the position $\boldsymbol{r}$. Thanks to this factorization, the time dependency in Eq. (4) can be dropped to yield the so-called **Helmholtz equation** for the propagation of $u(\boldsymbol{r})$:

$$\boxed{\big(\nabla^2 + k^2\big) u(\boldsymbol{r}) = 0} \tag{6}$$

with $k = 2\, \pi\, n\, \nu / c = 2\, \pi / \lambda$ the wave-number, $\lambda = c/(n\, \nu)$ the wavelength in the medium, and $\nabla^2 u = \partial^2 u / \partial x^2 + \partial^2 u / \partial y^2 + \partial^2 u / \partial z^2$ the Laplacian of u.

1.2 Elementary solutions to the Helmholtz equation

Before considering the diffraction by a surface, two important elementary solutions to the Helmholtz equation, the plane and spherical waves, are described here.

1.2.1 Plane wave

With the convention in Eq. (5), the field produced by a plane wave writes:

$$U(\boldsymbol{r}, t) = a\, \mathrm{Re}\Big(\mathrm{e}^{\mathrm{i}\, \boldsymbol{k} \cdot \boldsymbol{r} - \mathrm{i}\, 2\, \pi\, \nu\, t}\Big) \tag{7}$$

with $a = U(\boldsymbol{0}, 0)$ and $\boldsymbol{k} = (k_x, k_y, k_z)$ the wave-vector of amplitude $\|\boldsymbol{k}\| = k$ and whose direction is that of the propagation of the wave. The corresponding complex amplitude is:

$$u(\boldsymbol{r}) = a\, \mathrm{e}^{\mathrm{i}\, \boldsymbol{k} \cdot \boldsymbol{r}}, \tag{8}$$

Notation	Description
n	Refractive index of the medium
c	Propagation speed in the void
ν	Temporal frequency of wave
$\lambda = c/(n\,\nu)$	Wavelength in the medium
$k = 2\,\pi/\lambda$	Wave number
$\boldsymbol{k} = (k_x, k_y, k_z)$	Wave vector (with $k_z > 0$)
$\boldsymbol{r} = (x, y, z)$	Position in 3-dimensional space
$\boldsymbol{x} = (x, y)$	Transverse position in a transverse plane
$\boldsymbol{\alpha} = (\alpha_x, \alpha_y)$	Spatial frequency
z	Position along the propagation axis
$u_z(\boldsymbol{x}) = u_z(x, y) = u(x, y, z)$	Field in a transverse plane
$\widetilde{u}_z(\boldsymbol{\alpha}) = \widetilde{u}_z(\alpha_x, \alpha_y)$	Angular spectrum, 2-dimensional Fourier transform of $u_z(\boldsymbol{x})$

Table 1: Notations. All coordinates are Cartesian coordinates with the convention that the z-axis, corresponding to the optical axis, is oriented so that z increases as the waves physically propagate.

whose Laplacian is:

$$\nabla^2 u(\boldsymbol{r}) = -\left(k_x^2 + k_y^2 + k_z^2\right) a\, \mathrm{e}^{\mathrm{i}\,\boldsymbol{k}\cdot\boldsymbol{r}} = -k^2\, u(\boldsymbol{r}) \tag{9}$$

hence a plane wave is solution of the Helmholtz equation (6).

1.2.2 Spherical wave

With the convention in Eq. (5), the field produced by a spherical wave writes:

$$U(\boldsymbol{r}, t) = a\,\mathrm{Re}\left(\frac{\mathrm{e}^{\mathrm{i}\,k\cdot\|\boldsymbol{r}-\boldsymbol{r}_0\| - \mathrm{i}\,2\,\pi\,\nu\,t}}{\|\boldsymbol{r}-\boldsymbol{r}_0\|}\right) \tag{10}$$

for some constant a and with $\boldsymbol{r}_0 = (x_0, y_0, z_0)$ the origin of the spherical wave. The factor in $1/\|\boldsymbol{r}-\boldsymbol{r}_0\|$ is to account for the dilution of the power with the radius of the sphere. Note that the expression is singular in $\boldsymbol{r} = \boldsymbol{r}_0$ where the field is not defined. The complex amplitude of the spherical wave is:

$$u(\boldsymbol{r}) = \frac{a}{\|\boldsymbol{r}-\boldsymbol{r}_0\|}\,\mathrm{e}^{\mathrm{i}\,k\cdot\|\boldsymbol{r}-\boldsymbol{r}_0\|}. \tag{11}$$

The derivatives in x of $u(\boldsymbol{r})$ with $\boldsymbol{r} = (x, y, z)$ are:

$$\frac{\partial u(\boldsymbol{r})}{\partial x} = \left(\frac{\mathrm{i}\,k}{\|\boldsymbol{r}-\boldsymbol{r}_0\|} - \frac{1}{\|\boldsymbol{r}-\boldsymbol{r}_0\|^2}\right)(x - x_0)\, u(\boldsymbol{r}), \tag{12}$$

$$\frac{\partial^2 u(\boldsymbol{r})}{\partial x^2} = \left(\frac{\mathrm{i}\,k}{\|\boldsymbol{r}-\boldsymbol{r}_0\|} - \frac{3\,\mathrm{i}\,k\,(x-x_0)^2}{\|\boldsymbol{r}-\boldsymbol{r}_0\|^3} - \frac{k^2\,(x-x_0)^2}{\|\boldsymbol{r}-\boldsymbol{r}_0\|^2} - \frac{1}{\|\boldsymbol{r}-\boldsymbol{r}_0\|^2} + \frac{3\,(x-x_0)^2}{\|\boldsymbol{r}-\boldsymbol{r}_0\|^4}\right) u(\boldsymbol{r}), \tag{13}$$

and similar expressions for the derivatives in y and z. Combining the second derivatives yields:

$$\nabla^2 u(\boldsymbol{r}) = -k^2\, u(\boldsymbol{r}) \tag{14}$$

showing that a spherical wave is solution of the Helmholtz equation (6).

1.3 The Helmholtz equation for the modulation of a carrier wave

The field $u(\boldsymbol{r})$, with $\boldsymbol{r} \equiv (x, y, z)$, can be expressed as:

$$u(\boldsymbol{r}) = a(\boldsymbol{r})\, b(\boldsymbol{r}), \tag{15}$$

with $a(\boldsymbol{r})$ an unknown modulation field and $b(\boldsymbol{r})$ a chosen carrier wave. The second derivatives of $u(\boldsymbol{r})$ in x then write:

$$\frac{\partial^2 u}{\partial x^2} = \frac{\partial^2 a}{\partial x^2}\, b + 2\, \frac{\partial a}{\partial x}\, \frac{\partial b}{\partial x} + a\, \frac{\partial^2 b}{\partial x^2} \tag{16}$$

and similarly for the second derivatives in y and in z. Applying the Helmholtz equation (6) for $u(\boldsymbol{r})$ yields:

$$b\, \nabla^2 a + 2\, \boldsymbol{\nabla} a \cdot \boldsymbol{\nabla} b + a\, \left(\nabla^2 b + k^2\, b\right) = 0, \tag{17}$$

where $\boldsymbol{\nabla} a = \partial a / \partial \boldsymbol{r} = (\partial a/\partial x, \partial a/\partial y, \partial a/\partial z)$ denotes the spatial gradient of $a(\boldsymbol{r})$. Assuming now that the Helmholtz equation (6) holds for the carrier wave $b(\boldsymbol{r})$, i.e. $\nabla^2 b + k^2\, b = 0$, the Helmholtz equation for $u(\boldsymbol{r}) = a(\boldsymbol{r})\, b(\boldsymbol{r})$ is equivalent to:

$$\boxed{b(\boldsymbol{r})\, \nabla^2 a(\boldsymbol{r}) + 2\, \boldsymbol{\nabla} a(\boldsymbol{r}) \cdot \boldsymbol{\nabla} b(\boldsymbol{r}) = 0.} \tag{18}$$

This trick can be used to approximate the propagation of the auxiliary field $a(\boldsymbol{r})$ by a simpler differential equation, compared to the Helmholtz equation for $u(\boldsymbol{r})$, because the most significant spatial variations of the field $u(\boldsymbol{r})$ are taken into account by the carrier wave $b(\boldsymbol{r})$. We illustrate this by two examples.

As a first example, we choose the carrier beam to be a plane wave, see Eq. (8), which yields:

$$b(\boldsymbol{r}) = \mathrm{e}^{\mathrm{i}\, \boldsymbol{k} \cdot \boldsymbol{r}} \quad \Longrightarrow \quad \boldsymbol{\nabla} b(\boldsymbol{r}) = \mathrm{i}\, \boldsymbol{k}\, b(\boldsymbol{r}), \tag{19}$$

and Eq. (18) simplifies to:

$$\nabla^2 a + 2\, \mathrm{i}\, \boldsymbol{k} \cdot \boldsymbol{\nabla} a = 0. \tag{20}$$

is the equivalent Helmholtz equation for the auxiliary modulation field $a(\boldsymbol{r})$. It may be noted that the term $\boldsymbol{k} \cdot \boldsymbol{\nabla} a$ is k times the spatial derivative of $a(\boldsymbol{r})$ along the direction of propagation of the chosen carrier wave. This particular choice is made in Sec. **??** to derive the so-called paraxial approximation of the Helmholtz equation.

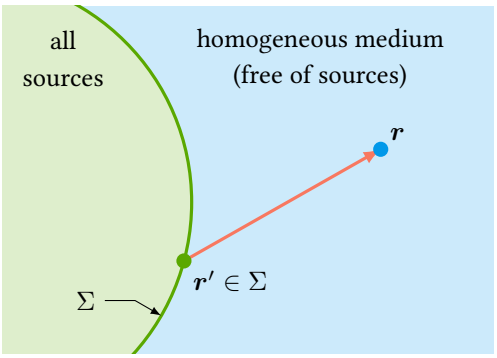

Figure 1: Boundary conditions for the diffraction by a surface. The field $u(\boldsymbol{r}')$ is assumed known at a surface Σ splitting space in 2 parts: all sources are on one side (in green), the other side is homogeneous medium (in blue). The light is propagating (orange arrow) from $\boldsymbol{r}' \in \Sigma$ to $\boldsymbol{r}$ in the homogeneous medium.

As a second example, we choose the carrier beam to be a spherical wave originating at $\boldsymbol{r}_0$, see Eq. (11), which yields:

$$b(\boldsymbol{r}) = \frac{\mathrm{e}^{\mathrm{i}\,k\,\|\boldsymbol{r}-\boldsymbol{r}_0\|}}{\|\boldsymbol{r}-\boldsymbol{r}_0\|} \quad \Longrightarrow \quad \boldsymbol{\nabla} b(\boldsymbol{r}) = \left(\frac{\mathrm{i}\,k}{\|\boldsymbol{r}-\boldsymbol{r}_0\|} - \frac{1}{\|\boldsymbol{r}-\boldsymbol{r}_0\|^2} \right) (\boldsymbol{r}-\boldsymbol{r}_0)\, b(\boldsymbol{r}), \tag{21}$$

and Eq. (18) simplifies to:

$$\nabla^2 a + 2 \left(\frac{\mathrm{i}\,k}{\|\boldsymbol{r}-\boldsymbol{r}_0\|} - \frac{1}{\|\boldsymbol{r}-\boldsymbol{r}_0\|^2} \right) (\boldsymbol{r}-\boldsymbol{r}_0) \cdot \boldsymbol{\nabla} a = 0. \tag{22}$$

is the equivalent Helmholtz equation for the auxiliary modulation field $a(\boldsymbol{r})$. It may be noted that the term $(\boldsymbol{r}-\boldsymbol{r}_0) \cdot \boldsymbol{\nabla} a$ is $\|\boldsymbol{r}-\boldsymbol{r}_0\|$ times the spatial derivative of $a(\boldsymbol{r})$ along the direction of propagation of the chosen carrier wave. Very far from $\boldsymbol{r}_0$, the spherical wave is approximately planar and it can be verified that Eq. (22) becomes indeed equivalent to Eq. (20).

1.4 Diffraction by a surface

To determine the field $u(\boldsymbol{r})$ at position $\boldsymbol{r}$ caused by given sources and using the Helmholtz equation (6), boundary conditions are needed. To that end, we may assume known the field at a closed surface Σ such that all considered sources are inside the volume delimited by Σ while $\boldsymbol{r}$ is outside this volume. Σ may also be an infinite surface splitting the space in two with the sources on one side of Σ and $\boldsymbol{r}$ on the other side. Figure 1 shows such boundary conditions. Solving the Helmholtz equation for $u(\boldsymbol{r})$ with such boundary conditions amounts to propagating the field from Σ to $\boldsymbol{r}$. All considered sources being *behind* Σ from the point of view of $\boldsymbol{r}$ and the Helmholtz equation being linear in the propagating field, the resulting field at $\boldsymbol{r}$ must be a linear

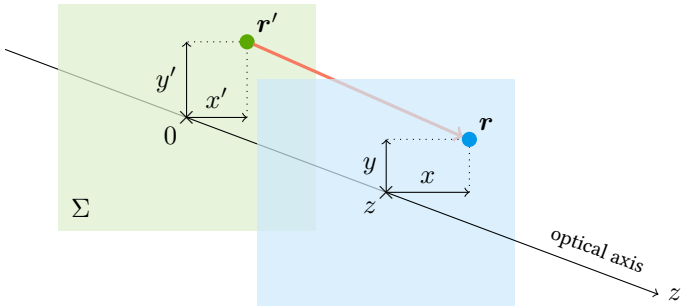

Figure 2: Diffraction by a planar surface. The transverse plane (in green) at position $z = 0$ along the optical axis is the surface Σ where the field is known.

combination of all contributions from the *emitting surface* Σ:

$$u(\boldsymbol{r}) = \iint_{\boldsymbol{r}' \in \Sigma} h(\boldsymbol{r}, \boldsymbol{r}')\, u(\boldsymbol{r}')\, \mathrm{d}^2\Sigma, \tag{23}$$

where $h(\boldsymbol{r}, \boldsymbol{r}')$ is a **propagation kernel**.

1.5 Diffraction by a planar surface

Many simplifications occur if the surface Σ is planar. If this is not the case, Kirchhoff diffraction equation can still be used (Goodman, 1996) but is really not suitable for fast computations. In the following, we develop the theory for a wave diffracted by a planar surface. This amounts to dealing with the **angular spectrum** for which solutions to the Helmholtz equation are quite easy to compute. Without demonstrating it, a solution for the field $u(\boldsymbol{r})$ provided by the type I **Rayleigh-Sommerfeld diffraction integral** is presented next for comparison.

1.5.1 Planar diffraction seen as a convolution

We consider the case where Σ is an infinite plane and call **optical axis** the perpendicular to Σ oriented in the direction of the physical propagation of waves (see Fig. 2). Without loss of generality, we choose the Cartesian coordinate system to be such that the z-axis coincides with the optical axis and the position of the transverse plane Σ is at the origin along this axis. In other words, the wave vector $\boldsymbol{k} = (k_x, k_y, k_z)$ of any propagating wave is such that $k_z > 0$. Since the space between Σ and $\boldsymbol{r}$ is homogeneous and devoid of sources, propagation between $\boldsymbol{r}' \in \Sigma$ and $\boldsymbol{r}$ shall only depend on the relative position $\boldsymbol{r} - \boldsymbol{r}'$. In other words, the propagation kernel must be **shift-invariant** and Eq. (23) becomes:

$$u(\boldsymbol{r}) = \iint h(\boldsymbol{r} - \boldsymbol{r}')\, u(\boldsymbol{r}')\, \mathrm{d}x'\, \mathrm{d}y', \tag{24}$$

where $(x', y', 0)$ are the Cartesian coordinates of $\boldsymbol{r}' \in \Sigma$. At this point, it is useful to introduce:

$$u_z(\boldsymbol{x}) = u_z(x, y) \equiv u(x, y, z) \tag{25}$$

to express the field $u(\boldsymbol{r})$ in a **transverse plane** of the optical axis as a 2-dimensional function of $\boldsymbol{x} = (x, y)$, the transverse position in this plane. Hereinafter, this notation will be used to emphasize that a function in a transverse plane at given z is considered. Using the same convention for the propagation kernel, Eq. (24) writes:

$$u_z(\boldsymbol{x}) = \iint h_z(\boldsymbol{x} - \boldsymbol{x}')\, u_0(\boldsymbol{x}')\, \mathrm{d}\boldsymbol{x}'. \tag{26}$$

In words, the diffracted field u_z in the transverse plane at z is the **2-dimensional convolution** of the field u_0 in the transverse plane Σ by a shift-invariant propagation kernel $h_z(\boldsymbol{x})$ between Σ and the transverse plane at z.

Clearly the propagation equation is unchanged by rotating the system around the optical axis, the propagation kernel shall therefore be a function of the transverse distance:

$$h_z(\boldsymbol{x}) = h_z(\|\boldsymbol{x}\|). \tag{27}$$

It can be checked that this property holds for the solutions found in the following.

1.5.2 The angular spectrum solution

The fact that the diffraction by a planar surface writes as a convolution in the transverse plane suggests to take the 2-dimensional Fourier transform of the complex amplitude $u_z(\boldsymbol{x})$ in the transverse plane at position z:

$$\widetilde{u}_z(\boldsymbol{\alpha}) \equiv \iint u_z(\boldsymbol{x})\, \mathrm{e}^{-\mathrm{i}\, 2\, \pi\, \boldsymbol{\alpha}\cdot\boldsymbol{x}}\, \mathrm{d}\boldsymbol{x} \tag{28}$$

with $\boldsymbol{\alpha} = (\alpha_x, \alpha_y)$ the Fourier spatial frequency conjugate to the position $\boldsymbol{x} = (x, y)$ in the transverse plane. For reasons given in Section 1.5.3, $\widetilde{u}_z(\boldsymbol{\alpha})$ is called the **angular spectrum**. The inverse Fourier transform of the angular spectrum gives back the field:

$$u_z(\boldsymbol{x}) = \iint \widetilde{u}_z(\boldsymbol{\alpha})\, \mathrm{e}^{+\mathrm{i}\, 2\, \pi\, \boldsymbol{\alpha}\cdot\boldsymbol{x}}\, \mathrm{d}\boldsymbol{\alpha}. \tag{29}$$

Taking the 2-dimensional Fourier transform of both sides of Eq. (26), the propagation of the Fourier transform of the field from the transverse plane Σ at the origin to the transverse plane at z simplifies to:

$$\boxed{\widetilde{u}_z(\boldsymbol{\alpha}) = \widetilde{h}_z(\boldsymbol{\alpha})\, \widetilde{u}_0(\boldsymbol{\alpha})} \tag{30}$$

with $\widetilde{h}_z(\boldsymbol{\alpha})$ the *propagation transfer function*, that is the Fourier transform of $h_z(\boldsymbol{x})$, the planar propagation kernel from the transverse plane at position 0 and and the one at position z along the z-axis.

A number of properties that hold for the propagation transfer function $\widetilde{h}_z(\boldsymbol{\alpha})$ can be inferred without knowing its exact expression:

- **No propagation.** If $z = 0$, the field shall remain unchanged, hence necessarily:

$$\widetilde{h}_0(\boldsymbol{\alpha}) = 1, \quad \forall \boldsymbol{\alpha}. \tag{31}$$

- **Successive propagation steps.** We expect that propagation can be split in successive propagation steps with the same result. For this property to hold, it is sufficient that propagation along the optical axis by z and then by z' be the same as propagation by $z + z'$ whatever z and z'. In other words:

$$\widetilde{h}_z(\boldsymbol{\alpha})\, \widetilde{h}_{z'}(\boldsymbol{\alpha}) = \widetilde{h}_{z+z'}(\boldsymbol{\alpha}), \quad \forall \boldsymbol{\alpha}, z, z'. \tag{32}$$

- **Reverse propagation.** Assuming the propagation transfer function is non-zero, the propagation in Eq. (30) can be inverted to recover the Fourier transform of the field in the transverse plane at the origin given the Fourier transform of the field in the transverse plane at z:

$$\widetilde{u}_0(\boldsymbol{\alpha}) = \frac{\widetilde{u}_z(\boldsymbol{\alpha})}{\widetilde{h}_z(\boldsymbol{\alpha})}.$$

  Besides, just exchanging longitudinal positions 0 and z in the reasoning leading to Eq. (30) yields:

$$\widetilde{u}_0(\boldsymbol{\alpha}) = \widetilde{h}_{-z}(\boldsymbol{\alpha})\, \widetilde{u}_z(\boldsymbol{\alpha}).$$

  These two relations must hold whatever the propagated field and the transverse positions and z, hence necessarily:

$$\widetilde{h}_{-z}(\boldsymbol{\alpha}) = \left(\widetilde{h}_z(\boldsymbol{\alpha})\right)^{-1}, \quad \forall \boldsymbol{\alpha}, z. \tag{33}$$

It can be noted that, if the propagation transfer function takes the form:

$$\widetilde{h}_z(\boldsymbol{\alpha}) = \mathrm{e}^{z\, \psi(\boldsymbol{\alpha})} \tag{34}$$

for any function $\psi\colon \mathbb{R}^2 \to \mathbb{C}$, then the properties (31), (32), and (33) hold as can be easily verified.

The expression of $\widetilde{h}_z(\boldsymbol{\alpha})$ can be obtained by solving the Helmholtz equation for the Fourier transform of the field. The following spatial derivatives of the field $u_z(\boldsymbol{x})$ can be obtained from Eq. (29) with $\boldsymbol{\alpha} = (\alpha_x, \alpha_y)$ and $\boldsymbol{x} = (x, y)$:

$$\frac{\partial^m u_z(\boldsymbol{x})}{\partial x^m} = (i\, 2\, \pi)^m \iint \widetilde{u}_z(\boldsymbol{\alpha})\, \alpha_x^m\, \mathrm{e}^{+\mathrm{i}\, 2\, \pi\, \boldsymbol{\alpha} \cdot \boldsymbol{x}}\, \mathrm{d}\boldsymbol{\alpha}, \tag{35}$$

$$\frac{\partial^m u_z(\boldsymbol{x})}{\partial y^m} = (i\, 2\, \pi)^m \iint \widetilde{u}_z(\boldsymbol{\alpha})\, \alpha_y^m\, \mathrm{e}^{+\mathrm{i}\, 2\, \pi\, \boldsymbol{\alpha} \cdot \boldsymbol{x}}\, \mathrm{d}\boldsymbol{\alpha}, \tag{36}$$

$$\frac{\partial^m u_z(\boldsymbol{x})}{\partial z^m} = \iint \frac{\partial^m \widetilde{u}_z(\boldsymbol{\alpha})}{\partial z^m}\, \mathrm{e}^{+\mathrm{i}\, 2\, \pi\, \boldsymbol{\alpha} \cdot \boldsymbol{x}}\, \mathrm{d}\boldsymbol{\alpha}, \tag{37}$$

for any $m \in \mathbb{N}$. Using these expressions (with $m = 2$) and applying the Helmholtz equation (6) to the field $u_z(\boldsymbol{x})$ given in Eq. (29) yields the equation of propagation for the Fourier transform of the field:

$$k^2 \left(1 - \|\lambda\, \boldsymbol{\alpha}\|^2\right) \widetilde{u}_z(\boldsymbol{\alpha}) + \frac{\partial^2 \widetilde{u}_z(\boldsymbol{\alpha})}{\partial z^2} = 0. \tag{38}$$

Remarkably, the Helmholtz equation is much simpler for the Fourier transform of the field than for the field because it only presents derivatives along z. In effect, by using the Fourier transform, the partial derivatives along the transverse coordinates have been replaced by simple multiplications by powers of the spatial frequencies.

Integrating Eq. (38) for z from 0 to z gives the following general solution for the Fourier transform of the field in the transverse plane at z:

$$\widetilde{u}_z(\boldsymbol{\alpha}) = \begin{cases} a_+(\boldsymbol{\alpha})\,\mathrm{e}^{+\mathrm{i}\,k\,z\,\sqrt{1-\|\lambda\,\boldsymbol{\alpha}\|^2}} \\ \quad + a_-(\boldsymbol{\alpha})\,\mathrm{e}^{-\mathrm{i}\,k\,z\,\sqrt{1-\|\lambda\,\boldsymbol{\alpha}\|^2}} & \text{if } \|\lambda\,\boldsymbol{\alpha}\| \leq 1, \\ a_+(\boldsymbol{\alpha})\,\mathrm{e}^{+k\,z\,\sqrt{\|\lambda\,\boldsymbol{\alpha}\|^2-1}} \\ \quad + a_-(\boldsymbol{\alpha})\,\mathrm{e}^{-k\,z\,\sqrt{\|\lambda\,\boldsymbol{\alpha}\|^2-1}} & \text{if } \|\lambda\,\boldsymbol{\alpha}\| > 1, \end{cases} \tag{39}$$

where $a_+(\boldsymbol{\alpha})$ and $a_-(\boldsymbol{\alpha})$ are functions to be determined by the boundary conditions. Taking $z = 0$ in both hand-sides of the general solution in Eq. (39) yields the boundary conditions in Σ:

$$a_+(\boldsymbol{\alpha}) + a_-(\boldsymbol{\alpha}) = \widetilde{u}_0(\boldsymbol{\alpha}). \tag{40}$$

According to our convention that z increases as the waves physically propagate, then:

- $z > 0$ corresponds to **forward propagation**, *i.e.* the wave is physically propagating from the transverse plane Σ to the one at z;
- $z < 0$ corresponds to **reverse propagation**.

To eliminate un-physical solutions, we consider the case of forward propagation, *i.e.* $z > 0$. There are two regimes to examine:

- If $\|\lambda\,\boldsymbol{\alpha}\| \leq 1$, the convention in Eq. (5) implies that the phase of the propagating wave is increasing with the distance of propagation, hence $a_-(\boldsymbol{\alpha}) = 0$ and, from Eq. (40), $a_+(\boldsymbol{\alpha}) = \widetilde{u}_0(\boldsymbol{\alpha})$. The solution then writes:

$$\widetilde{u}_z(\boldsymbol{\alpha}) = \widetilde{u}_0(\boldsymbol{\alpha})\,\mathrm{e}^{\mathrm{i}\,k\,z\,\sqrt{1-\|\lambda\,\boldsymbol{\alpha}\|^2}}. \tag{41}$$

- If $\|\lambda\,\boldsymbol{\alpha}\| > 1$, the amplitude of the wave must not increase with the distance of propagation, hence $a_+(\boldsymbol{\alpha}) = 0$ and, from Eq. (40), $a_-(\boldsymbol{\alpha}) = \widetilde{u}_0(\boldsymbol{\alpha})$. The solution then writes:

$$\widetilde{u}_z(\boldsymbol{\alpha}) = \widetilde{u}_0(\boldsymbol{\alpha})\,\mathrm{e}^{-k\,z\,\sqrt{\|\lambda\,\boldsymbol{\alpha}\|^2-1}}. \tag{42}$$

  This high frequencies regime corresponds to **evanescent waves** that are rapidly vanishing with z, the distance of propagation. In words, no spatial frequencies higher than $1/\lambda$ are propagating.

Combining these solutions with Eq. (30), the transfer function implementing the propagation between transverse planes for the Fourier transform of the field writes:

$$\widetilde{h}_z(\boldsymbol{\alpha}) = \begin{cases} \exp\left(\mathrm{i}\,k\,z\,\sqrt{1-\|\lambda\,\boldsymbol{\alpha}\|^2}\right) & \text{if } \|\lambda\,\boldsymbol{\alpha}\| \leq 1, \\ \exp\left(-k\,z\,\sqrt{\|\lambda\,\boldsymbol{\alpha}\|^2-1}\right) & \text{if } \|\lambda\,\boldsymbol{\alpha}\| > 1. \end{cases} \tag{43}$$

High-frequencies, *i.e.* $\|\lambda\,\boldsymbol{\alpha}\| > 1$, which correspond to evanescent waves can be neglected except for short propagation distances. A more synthetic expression of Eq. (43) is provided by:

$$\boxed{\widetilde{h}_z(\boldsymbol{\alpha}) = \mathrm{e}^{\mathrm{i}\,k\,z\,\sqrt{1-\|\lambda\,\boldsymbol{\alpha}\|^2}}} \tag{44}$$

which holds for $\|\boldsymbol{\alpha}\| \leq 1/\lambda$ and for $\|\boldsymbol{\alpha}\| > 1/\lambda$ with the usual convention that $\sqrt{t} = \mathrm{i}\,\sqrt{-t}$ when $t < 0$.

The transfer function in Eq. (44) has the exponential form envisioned in Eq. (34), hence the properties (31), (32), and (33) do hold for $\widetilde{h}_z(\boldsymbol{\alpha})$. In particular, the reverse propagation property in Eq. (33) which means that the theory is consistent for forward ($z > 0$) and reverse ($z < 0$) propagation. The expression of the propagation transfer function in Eq. (44) is therefore valid whatever the sign of z. As shown later, this is not the case for the Rayleigh-Sommerfeld diffraction integral presented in Section 1.5.4.

1.5.3 Interpretation of the angular spectrum

Combining Eqs. (29), (30), and (44), the field in the transverse plane at position $z > 0$ knowing (the Fourier transform of) the field in the transverse plane Σ at $z = 0$ writes:

$$\begin{aligned} u_z(\boldsymbol{x}) &= \iint \widetilde{u}_0(\boldsymbol{\alpha})\,\widetilde{h}_z(\boldsymbol{\alpha})\,\mathrm{e}^{+\mathrm{i}\,2\,\pi\,\boldsymbol{\alpha}\cdot\boldsymbol{x}}\,\mathrm{d}\boldsymbol{\alpha} \\ &= \iint \widetilde{u}_0(\boldsymbol{\alpha})\,\mathrm{e}^{+\mathrm{i}\left(2\,\pi\,\boldsymbol{\alpha}\cdot\boldsymbol{x}+k\,z\,\sqrt{1-\|\lambda\,\boldsymbol{\alpha}\|^2}\right)}\,\mathrm{d}\boldsymbol{\alpha}. \end{aligned} \tag{45}$$

The phase of the complex exponential in Eq. (45) can be rewritten as:

$$2\,\pi\,\boldsymbol{\alpha}\cdot\boldsymbol{x} + k\,z\,\sqrt{1-\|\lambda\,\boldsymbol{\alpha}\|^2} = \langle \boldsymbol{k}(\boldsymbol{\alpha}), \boldsymbol{r}\rangle, \tag{46}$$

the scalar product of $\boldsymbol{r} = (x, y, z)$ and $\boldsymbol{k}(\boldsymbol{\alpha}) = (k_x(\boldsymbol{\alpha}), k_y(\boldsymbol{\alpha}), k_z(\boldsymbol{\alpha}))$ whose Cartesian coordinates are given by:

$$\begin{cases} \boldsymbol{k}_\perp(\boldsymbol{\alpha}) = (k_x(\boldsymbol{\alpha}), k_y(\boldsymbol{\alpha})) = 2\,\pi\,(\alpha_x, \alpha_y) = 2\,\pi\,\boldsymbol{\alpha}, \\ k_z(\boldsymbol{\alpha}) = k\,\sqrt{1-\|\lambda\,\boldsymbol{\alpha}\|^2}. \end{cases} \tag{47}$$

Using $\boldsymbol{k}(\boldsymbol{\alpha})$, Eq. (45) simplifies to:

$$u(\boldsymbol{r}) = u_z(\boldsymbol{x}) = \iint \widetilde{u}_0(\boldsymbol{\alpha})\,\mathrm{e}^{\mathrm{i}\,\boldsymbol{k}(\boldsymbol{\alpha})^\top\cdot\boldsymbol{r}}\,\mathrm{d}\boldsymbol{\alpha} \tag{48}$$

which is readily a superposition of plane waves of wave vector $\boldsymbol{k}(\boldsymbol{\alpha})$, see Eq. (8), weighted by $\widetilde{u}_0(\boldsymbol{\alpha})$. In this representation, the spatial frequencies multiplied by the wavelength, $\lambda\,\boldsymbol{\alpha}$, are the cosines of the angles of the wave-vector $\boldsymbol{k}(\boldsymbol{\alpha})$ with the transverse unit vectors $\boldsymbol{e}_x$ and $\boldsymbol{e}_y$. For that reason, the Fourier spectrum $\widetilde{u}_z(\boldsymbol{\alpha})$ is called the **angular spectrum** of the field in the transverse plane at z.

It can be easily shown that $\|\boldsymbol{k}(\boldsymbol{\alpha})\| = 2\,\pi/\lambda = k$, the wave-number, whatever the sign of $1 - \|\lambda\,\boldsymbol{\alpha}\|^2$ with the same convention for the square root of a negative number as assumed in Eq. (44). Hence all the plane waves in Eq. (48) have the same wavelength.

In the next section, one of the Rayleigh-Sommerfeld solution for the diffraction integral for the complex amplitude is given but obtaining this result is much more complex than via the angular spectrum. In Appendix A, the Helmholtz equation is solved assuming that the field is a superposition of plane waves. The obtained solution is, of course, the same but the initial assumption is not proven. Konijnenberg et al. (2022) propose another resolution of the Helmholtz equation directly based on the interpretation that the inverse Fourier transform of the angular spectrum, Eq. (29), is a superposition of plane waves for which the propagation is known, *cf.* Eq. (8).

1.5.4 Rayleigh-Sommerfeld diffraction

The field in a transverse plane at $z > 0$ caused by the diffraction of the field in a finite size aperture $\mathcal{A}$ of the transverse plane Σ at[2] z' is given by the Rayleigh-Sommerfeld diffraction integrals. The first kind of these solutions writes (Born et al., 2002):

$$u(x,y,z) = \frac{1}{2\,\pi}\iint_{\mathcal{A}} u(x',y',z')\,\frac{\partial}{\partial z'}\left(\frac{\mathrm{e}^{\mathrm{i}\,k\,s}}{s}\right)\mathrm{d}x'\,\mathrm{d}y' \tag{49}$$

with $s = \sqrt{(x-x')^2 + (y-y')^2 + (z-z')^2}$ and for $z > z'$. Since $s = \|\boldsymbol{r} - \boldsymbol{r}'\|$, the term $\mathrm{e}^{\mathrm{i}\,k\,s}/s$ corresponds to a spherical wave proceeding from a source at $\boldsymbol{r}' = (x',y',z')$.

Rayleigh-Sommerfeld diffraction integral in Eq. (49) has the form of Eq. (23) whose propagation kernel can be computed as follows:

$$\begin{aligned} h\big((x,y,z),(x',y',z')\big) &= \frac{1}{2\,\pi}\,\frac{\partial}{\partial z'}\left(\frac{\mathrm{e}^{\mathrm{i}\,k\,s}}{s}\right) \\ &= \frac{1}{2\,\pi}\,\frac{\partial}{\partial s}\left(\frac{\mathrm{e}^{\mathrm{i}\,k\,s}}{s}\right)\frac{\partial s}{\partial z'} \\ &= \frac{1}{2\,\pi}\,\frac{\mathrm{e}^{\mathrm{i}\,k\,s}}{s}\left(\mathrm{i}\,k - \frac{1}{s}\right)\frac{z'-z}{s} \\ &= \frac{(z-z')\,\mathrm{e}^{\mathrm{i}\,k\,s}}{s^2}\left(\frac{1}{\mathrm{i}\,\lambda} + \frac{1}{2\,\pi\,s}\right) \end{aligned} \tag{50}$$

for $z > z'$ and $s = \sqrt{(x-x')^2 + (y-y')^2 + (z-z')^2}$. As predicted before for the diffraction by a planar surface, this function is shift-invariant and Rayleigh-Sommerfeld diffraction integral is a 2-dimensional convolution in the transverse plane Σ.

Using the notation of Eq. (26) and the convention that Σ is at $z' = 0$, Rayleigh-

[2] in the remaining it is needed to explicitely introduce the longitidinal position z' of Σ because derivative with respect to z' has to be taken

Sommerfeld propagation kernel simplifies to:

$$h_z(\boldsymbol{x}) = \frac{z\,\mathrm{e}^{\mathrm{i}\,k\,r}}{r^2}\left(\frac{1}{\mathrm{i}\,\lambda} + \frac{1}{2\,\pi\,r}\right) \tag{51}$$

with $\boldsymbol{x} = (x, y)$, $z > 0$, $r = \sqrt{\|\boldsymbol{x}\|^2 + z^2}$ the distance of propagation, and λ the wavelength in the propagation medium. The term $1/(2\,\pi\,r)$ accounts for evanescent waves and can be neglected at propagating distances longer than a few wavelengths.

Long after Rayleigh (1897) and Sommerfeld (1896) had found the solution (49) to the diffraction by a planar surface, Lalor (1968) (at Emil Wolf's instigation) rigorously proved that the inverse Fourier transform of the angular spectrum transfer function $\widetilde{h}_z(\boldsymbol{\alpha})$ given in Eq. (44) was indeed the propagation kernel $h_z(\boldsymbol{x})$ given in Eq. (51) provided $z \geq 0$, that is for forward propagation.

Angular spectrum progation, or Rayleigh-Sommerfeld diffraction, amounts to performing a 2-dimensional convolution. The numerical application of this kind of planar propagation are discussed in Section 2.2. In the next section, we introduce an approximation that yields simpler equations for planar propagation.

1.6 Paraxial approximation: Fresnel diffraction

Fresnel diffraction is an approximation of the diffraction by a planar surface when the so-called **paraxial conditions** hold. These conditions are satisfied in the following cases (which are all equivalent):

- the high frequencies of the angular spectrum are negligible;
- the variations of the complex amplitude along the direction perpendicular to the surface can be well approximated by those of a plane wave;
- diffracted waves have small propagation angles with the normal to the diffracting surface.

Fresnel diffraction is important because the above conditions correspond to many common practical cases and because it yields equations that are well adapted to fast numeric computations (*i.e.* integrals can be evaluated by means of FFTs). The Fresnel approximation of the diffraction can be obtained from any of the above conditions. We start by the angular spectrum which (again) is the most straightforward and consistent path to follow. The other approaches are considered next.

1.6.1 The angular spectrum transfer function at low frequencies

If the angular spectrum $\widetilde{u}_z(\boldsymbol{\alpha})$ is only significant at low frequencies such that $\|\boldsymbol{\alpha}\| \ll 1/\lambda$, then, to apply the angular spectrum propagation in Eq. (30), the term $\sqrt{1 - \|\lambda\,\boldsymbol{\alpha}\|^2}$ in the propagation transfer function $\widetilde{h}_z(\boldsymbol{\alpha})$ in Eq. (44) can be approximated using the Taylor's series:

$$\sqrt{1 - \|\lambda\,\boldsymbol{\alpha}\|^2} = 1 - \frac{\|\lambda\,\boldsymbol{\alpha}\|^2}{2} - \frac{\|\lambda\,\boldsymbol{\alpha}\|^4}{8} - \frac{\|\lambda\,\boldsymbol{\alpha}\|^6}{16} - \dots \tag{52}$$

This leads to the following approximation for $\|\lambda\,\boldsymbol{\alpha}\| \ll 1$:

$$\widetilde{h}_z(\boldsymbol{\alpha}) = \mathrm{e}^{\mathrm{i}\,k\,z\,\sqrt{1-\|\lambda\,\boldsymbol{\alpha}\|^2}} \approx \mathrm{e}^{\mathrm{i}\,k\,z\,\left[1-\frac{1}{2}\,\|\lambda\,\boldsymbol{\alpha}\|^2\right]}. \tag{53}$$

However, the omitted terms in the series must be small compared to $\|\lambda\,\boldsymbol{\alpha}\|^2/2$ but also such that they can only produce a phase change much smaller than $2\,\pi$, hence considering the largest (in magnitude) of the omitted terms, the following must hold:

$$k\,|z|\,\frac{\|\lambda\,\boldsymbol{\alpha}\|^4}{8} \ll 2\,\pi \quad \Longrightarrow \quad \|\lambda\,\boldsymbol{\alpha}\| \ll (8\,\lambda/|z|)^{1/4}. \tag{54}$$

Finally, the paraxial approximation of the angular spectrum propagation transfer function is given by:

$$\boxed{\widetilde{h}_z(\boldsymbol{\alpha}) = \mathrm{e}^{\mathrm{i}\,\left(k-\pi\,\lambda\,\|\boldsymbol{\alpha}\|^2\right)\,z} \quad \text{for } \|\lambda\,\boldsymbol{\alpha}\| \ll \min\left[1, (8\,\lambda/|z|)^{1/4}\right]} \tag{55}$$

with λ the wavelength in the medium and z the (algebraic) propagation distance. It is worth noting that this transfer function has the exponential form given in Eq. (34), hence the properties (31), (32), and (33) do hold for the paraxial approximation of $\widetilde{h}_z(\boldsymbol{\alpha})$. If $\boldsymbol{\alpha} \neq \mathbf{0}$, all omitted terms in the Taylor's series of $\sqrt{1-\|\lambda\,\boldsymbol{\alpha}\|^2}$ are negative and, thus, the paraxial approximation systematically underestimates the phase change due to the propagation. In general, $|z| \gg \lambda$, so the paraxial conditions for the frequencies simplifies to $\|\lambda\,\boldsymbol{\alpha}\| \ll (8\,\lambda/|z|)^{1/4}$.

In order to derive a closed-form expression of the propagation kernel $h_z(\boldsymbol{x})$ in the paraxial conditions, we need to generalize the (inverse) Fourier transform of a 2-dimensional Gaussian shaped function:

$$\boxed{\iint \mathrm{e}^{-\pi\,q\,\|\boldsymbol{x}\|^2}\,\mathrm{e}^{\pm\mathrm{i}\,2\,\pi\,\boldsymbol{x}\cdot\boldsymbol{\alpha}}\,\mathrm{d}\boldsymbol{x} = \frac{\mathrm{e}^{-\frac{\pi}{q}\,\|\boldsymbol{\alpha}\|^2}}{q}} \tag{56}$$

which is also a Gaussian shaped function. Equation (56) holds for any $q > 0$. By analytic continuation, we assume that it also holds for any $q \in \mathbb{C}^\star$ such that $\mathrm{Re}(q) \geq 0$. In particular[3], taking $q = \mathrm{i}\,\rho$ with $\rho \in \mathbb{R}^\star$ in Eq. (56) yields the (inverse) Fourier transform of a 2-dimensional quadratic phase factor:

$$\iint \mathrm{e}^{-\mathrm{i}\,\pi\,\rho\,\|\boldsymbol{x}\|^2}\,\mathrm{e}^{\pm\mathrm{i}\,2\,\pi\,\boldsymbol{x}\cdot\boldsymbol{\alpha}}\,\mathrm{d}\boldsymbol{x} = \frac{\mathrm{e}^{\frac{\mathrm{i}\,\pi}{\rho}\,\|\boldsymbol{\alpha}\|^2}}{\mathrm{i}\,\rho} \tag{57}$$

which is also a quadratic phase factor. Using Eq. (57), the inverse Fourier transform of the propagation transfer function given in Eq. (55) can be computed to yield the propagation kernel in the paraxial approximation:

$$\boxed{h_z(\boldsymbol{x}) = \frac{\mathrm{e}^{\mathrm{i}\,2\,\pi\,z/\lambda}}{\mathrm{i}\,\lambda\,z}\,\mathrm{e}^{\frac{\mathrm{i}\,\pi\,\|\boldsymbol{x}\|^2}{\lambda\,z}} = \frac{\mathrm{e}^{\mathrm{i}\,k\,z}}{\mathrm{i}\,\lambda\,z}\,\mathrm{e}^{\frac{\mathrm{i}\,k\,\|\boldsymbol{x}\|^2}{2\,z}}.} \tag{58}$$

[3]The more general case of $q \in \mathbb{C}^\star$ such that $\mathrm{Re}(q) \geq 0$ is suitable to derive the equations of propagation for a Gaussian beam.

As shown next, the condition $\|\boldsymbol{\alpha}\| \ll 1/\lambda$ for Eq. (55) is equivalent to $\|\boldsymbol{x}\| \ll |z|$ for Eq. (58). Propagation by this kernel implements Fresnel diffraction expressed by the **Fresnel diffraction integral**:

$$\boxed{u_z(\boldsymbol{x}) = \frac{\mathrm{e}^{\mathrm{i}\,k\,z}}{\mathrm{i}\,\lambda\,z} \iint u_0(\boldsymbol{x}')\,\mathrm{e}^{\frac{\mathrm{i}\,\pi\,\|\boldsymbol{x}-\boldsymbol{x}'\|^2}{\lambda\,z}}\,\mathrm{d}\boldsymbol{x}'.} \tag{59}$$

1.6.2 Modulation of a plane carrier wave

The field $u(x, y, z)$ can be expressed as a modulation of a chosen carrier wave. Assuming that the carrier wave is a plane wave whose wave vector is $\boldsymbol{k} = k\,\boldsymbol{e}_z$, the field can be expressed as:

$$u(x, y, z) = a(x, y, z)\,\mathrm{e}^{\mathrm{i}\,k\,z}, \tag{60}$$

with $a(x, y, z)$ the modulation field. Using this above expression, the derivatives of $u(x, y, z)$ are:

$$\frac{\partial^2 u(x,y,z)}{\partial x^2} = \frac{\partial^2 a(x,y,z)}{\partial x^2}\,\mathrm{e}^{\mathrm{i}\,k\,z}, \tag{61}$$

$$\frac{\partial^2 u(x,y,z)}{\partial y^2} = \frac{\partial^2 a(x,y,z)}{\partial y^2}\,\mathrm{e}^{\mathrm{i}\,k\,z}, \tag{62}$$

$$\frac{\partial u(x,y,z)}{\partial z} = \left(\frac{\partial a(x,y,z)}{\partial z} + \mathrm{i}\,k\,a(x,y,z)\right)\mathrm{e}^{\mathrm{i}\,k\,z}, \tag{63}$$

$$\frac{\partial^2 u(x,y,z)}{\partial z^2} = \left(\frac{\partial^2 a(x,y,z)}{\partial z^2} + 2\,\mathrm{i}\,k\,\frac{\partial a(x,y,z)}{\partial z} - k^2\,a(x,y,z)\right)\mathrm{e}^{\mathrm{i}\,k\,z}. \tag{64}$$

Using Eqs. (61), (62), and (64), the Helmholtz equation (6) for the modulation field $a(x, y, z)$ writes:

$$\left(\underbrace{\frac{\partial^2}{\partial x^2} + \frac{\partial^2}{\partial y^2} + \frac{\partial^2}{\partial z^2}}_{\nabla^2} + 2\,\mathrm{i}\,k\,\frac{\partial}{\partial z}\right) a(x, y, z) = 0. \tag{65}$$

In the **paraxial approximation**, it is assumed that the carrier plane wave explains most of the variations of the field along z and thus that the second derivative of the modulation $a(x, y, z)$ in z is negligible compared to the term involving the first derivative:

$$\left|\frac{\partial^2 a}{\partial z^2}\right| \ll \left|2\,k\,\frac{\partial a}{\partial z}\right| \quad\Longrightarrow\quad \left(\underbrace{\frac{\partial^2}{\partial x^2} + \frac{\partial^2}{\partial y^2}}_{\nabla_\perp^2} + 2\,\mathrm{i}\,k\,\frac{\partial}{\partial z}\right) a(x, y, z) = 0, \tag{66}$$

which is the **paraxial wave equation** for the modulation field $a(x, y, z)$. Multiplying by $\exp(\mathrm{i}\, k\, z)$ and using Eq. (63), the paraxial wave equation for the field writes[4]:

$$\left(\underbrace{\frac{\partial^2}{\partial x^2} + \frac{\partial^2}{\partial y^2}}_{\nabla_\perp^2} + 2\,\mathrm{i}\, k\, \frac{\partial}{\partial z} - 2\, k^2 \right) u(x, y, z) = 0. \tag{67}$$

Using the same notation as in Eq. (25) and the 2-dimensional Fourier in a transverse plane and its inverse defined in Eqs. (28) and (29), the paraxial wave equation for the Fourier transform of the modulation field writes:

$$\frac{\partial \widetilde{a}_z(\boldsymbol{\alpha})}{\partial z} = -\mathrm{i}\, \pi\, \lambda\, \|\boldsymbol{\alpha}\|^2\, \widetilde{a}_z(\boldsymbol{\alpha}). \tag{68}$$

Integration of this equation for from 0 to z yields:

$$\widetilde{a}_z(\boldsymbol{\alpha}) = \widetilde{a}_0(\boldsymbol{\alpha})\, \mathrm{e}^{-\mathrm{i}\, \pi\, \lambda\, z\, \|\boldsymbol{\alpha}\|^2}. \tag{69}$$

From Eq. (60) and by linearity of the transverse Fourier transform, it is easy to show that:

$$\widetilde{u}_z(\boldsymbol{\alpha}) = \widetilde{a}_z(\boldsymbol{\alpha})\, \mathrm{e}^{\mathrm{i}\, k\, z}, \tag{70}$$

and thus:

$$\widetilde{u}_z(\boldsymbol{\alpha}) = \widetilde{u}_0(\boldsymbol{\alpha})\, \mathrm{e}^{\mathrm{i}\, \left(k - \pi\, \lambda\, \|\boldsymbol{\alpha}\|^2\right) z}. \tag{71}$$

The transfer function in the above right-hand side is exactly the paraxial approximation of the angular spectrum propagation transfer function given in Eq. (55). Hence, the approximation of neglecting the second derivatives in z of the modulation field which leads to Eq. (66) is equivalent to the approximation $\sqrt{1 - \|\lambda\, \boldsymbol{\alpha}\|^2} \approx 1 - \|\lambda\, \boldsymbol{\alpha}\|^2/2$ that holds at low frequencies such that $\|\boldsymbol{\alpha}\| \ll 1/\lambda$ and used to obtain Eq. (55) more directly.

1.6.3 From Rayleigh-Sommerfeld diffraction to Fresnel diffraction

Finally, it is interesting to derive an expression of the propagation kernel in paraxial conditions by approximating the Rayleigh-Sommerfeld propagation kernel h_z, given in Eq. (51), for small diffraction angles and neglecting evanescent waves.

For small diffraction angles, that is for $\|\Delta\boldsymbol{x}\| \ll |z|$ with $\Delta\boldsymbol{x} = \boldsymbol{x} - \boldsymbol{x}'$, the following series can be used to approximate r the propagation distance used in Eq. (51):

$$\begin{aligned} r &= \sqrt{\|\Delta\boldsymbol{x}\|^2 + z^2} \\ &= |z|\, \sqrt{1 + \|\Delta\boldsymbol{x}/z\|^2} \\ &= |z| + \frac{\|\Delta\boldsymbol{x}\|^2}{2\,|z|} - \frac{\|\Delta\boldsymbol{x}\|^4}{8\,|z|^3} + \frac{\|\Delta\boldsymbol{x}\|^6}{16\,|z|^5} - \dots \end{aligned} \tag{72}$$

[4] in https://en.wikipedia.org/wiki/Helmholtz_equation#Paraxial_approximation a different solution is given without the k^2 term...

In the denominator of the right-hand side expression of Eq. (51), the first term of the series is sufficient but, in the complex exponential, at least the two first terms must be kept to account for the phase changes with the transverse position $\boldsymbol{x} = (x, y)$. More specifically, the third and subsequent terms of the series can be neglected in the $\mathrm{e}^{\mathrm{i}\,k\,r}$ term if the following condition holds:

$$\frac{\|\Delta\boldsymbol{x}\|^4}{8\,|z|^3} \ll \lambda \quad \Longleftrightarrow \quad \|\Delta\boldsymbol{x}\| \ll \left(8\,\lambda\,|z|^3\right)^{1/4} \tag{73}$$

which is another expression of the **paraxial conditions**[5]. If these conditions hold, the Rayleigh-Sommerfeld propagation kernel can be approximated by:

$$h_z(\Delta\boldsymbol{x}) \approx \frac{\exp\left(\mathrm{i}\,k\left[|z| + \frac{\|\Delta\boldsymbol{x}\|^2}{2\,|z|}\right]\right)}{\mathrm{i}\,\lambda\,z}$$

whose right-hand-side is the Fresnel propagation kernel given in Eq. (58) except that z is replaced by $|z|$ in the exponential function. The two expressions are only identical for $z \geq 0$ that is for *forward propagation*. Rayleigh-Sommerfeld theory is not suitable for *reverse propagation*.

1.6.4 Alternative formulation of Fresnel diffraction integral

The Fresnel diffraction integral in Eq. (59) has the form of a convolution which can be computed by 2 Fourier transforms using the expression of the propagation transfer function (or 3 Fourier transforms if the expression of the propagation kernel is used instead). As shown next, the Fresnel diffraction integral can also be computed by a single Fourier transform at the cost of a constraint linking the sampling steps for the two transverse planes.

Introducing the quadratic phase factor:

$$\mathcal{Q}_\rho(\boldsymbol{x}) = \exp\left(\mathrm{i}\,\pi\,\rho\,\|\boldsymbol{x}\|^2\right) \tag{74}$$

and developping the term $\|\boldsymbol{x} - \boldsymbol{x}'\|^2$ in the Fresnel propagation kernel given by Eq. (58), the field in the transverse plane at z can be written as:

$$u_z(\boldsymbol{x}) = \frac{\mathrm{e}^{\mathrm{i}\,k\,z}}{\mathrm{i}\,\lambda\,z}\,\mathcal{Q}_{\frac{1}{\lambda\,z}}(\boldsymbol{x}) \iint \left[u_0(\boldsymbol{x}')\,\mathcal{Q}_{\frac{1}{\lambda\,z}}(\boldsymbol{x}')\right] \mathrm{e}^{-\frac{\mathrm{i}\,2\,\pi}{\lambda\,z}\,\boldsymbol{x}\cdot\boldsymbol{x}'}\,\mathrm{d}\boldsymbol{x}', \tag{75}$$

which is known as the *Fresnel transform* of u_0. It can be noted that the 2-dimensional integral is the Fourier transform of the term inside the square brackets at the *frequency*[6] $\boldsymbol{\alpha} = \boldsymbol{x}/(\lambda\,|z|)$ if $z > 0$, its inverse Fourier transform if $z < 0$. This formula and the angular spectrum are two possible methods to numerically compute the propagation by means of fast Fourier transforms (FFTs). However, computing the Fresnel transform given by Eq. (75) by means of the FFT imposes that $\delta x_0\,\delta x_z = \lambda\,|z|/N$ with δx_0 and δx_z the respective sampling steps in the transverse plane at the origin and at z, and N the number of samples along a given transverse direction (see Sect. C).

[5] For a wavelength $\lambda = 500\,\mathrm{nm}$, the paraxial conditions in Eq. (73) correspond to a region of about 1 mm in radius at a propagation distance $z = 1\,\mathrm{cm}$.

[6] Interpreting $\boldsymbol{\alpha} = \boldsymbol{x}/(\lambda\,|z|)$ as a frequency, the paraxial conditions in Eq. (54), that $\|\lambda\,\boldsymbol{\alpha}\| \ll |8\,\lambda/z|^{1/4}$, and in Eq. (73), that $\|\boldsymbol{x}\| \ll |8\,\lambda\,z^3|^{1/4}$, are in fact the same conditions.

1.6.5 Planar wave in the paraxial approximation.

In the paraxial approximation, the wave-vector, $\boldsymbol{k} = (k_x, k_y, k_z)$, of a planar wave is such that $|k_x| \ll |k_z|$ and $|k_y| \ll |k_z|$. Hence and because of the choice of the orientation of the z-axis which implies that $k_z > 0$, $k_z \approx k$. Using the planar wave decomposition of Eq. (48), a planar wave in the paraxial approximation is approximated by:

$$u_z(x, y) \propto \mathrm{e}^{\,\mathrm{i}\left(\boldsymbol{k}_\perp \cdot \boldsymbol{x} + z\sqrt{k^2 - \|\boldsymbol{k}_\perp\|^2}\right)} \approx \mathrm{e}^{\,\mathrm{i}\,k\,z}\,\mathrm{e}^{\,\mathrm{i}\,\boldsymbol{k}_\perp \cdot \boldsymbol{x}} \tag{76}$$

with $\boldsymbol{k}_\perp = (k_x, k_y) = 2\,\pi\,\boldsymbol{\alpha}$ where $\boldsymbol{\alpha}$ is the spatial frequency of the angular spectrum of the planar wave.

1.6.6 Spherical wave in the paraxial approximation.

In the paraxial approximation, a spherical wave originating from $\boldsymbol{r}_0 = (x_0, y_0, z_0)$ becomes:

$$u_z(x, y) \propto \frac{\mathrm{e}^{\,\mathrm{i}\,k\,\|\boldsymbol{r} - \boldsymbol{r}_0\|}}{\|\boldsymbol{r} - \boldsymbol{r}_0\|} = \frac{\mathrm{e}^{\,\mathrm{i}\,k\,\sqrt{\|\boldsymbol{x} - \boldsymbol{x}_0\|^2 + \Delta z^2}}}{\sqrt{\|\boldsymbol{x} - \boldsymbol{x}_0\|^2 + \Delta z^2}} \approx \frac{\mathrm{e}^{\,\mathrm{i}\,k\left(|\Delta z| + \frac{\|\boldsymbol{x} - \boldsymbol{x}_0\|^2}{2\,|\Delta z|}\right)}}{|\Delta z|} \tag{77}$$

with $\boldsymbol{r} = (x, y, z)$, $\Delta z = z - z_0$, $\boldsymbol{x} = (x, y)$, and $\boldsymbol{x}_0 = (x_0, y_0)$. It may be noted that the right-hand side of Eq. (77) is equal to $(-\mathrm{i}/\lambda)\,h_{|\Delta z|}(\boldsymbol{x})$ with $h_{\Delta z}$ the Fresnel propagation kernel given in Eq. (58).

1.6.7 Propagation of Gaussian beams in the paraxial approximation

TBD

1.7 Fraunhofer diffraction

TBD

2 Propagation methods

Equipped with the equations of propagation, we can now consider how to use them for modeling optical propagation. There are several possible fast methods[7] to propagate the field:

- **Propagation by discrete convolution.** This method consists in approximating the diffraction integral in Eq. (26) by a 2-dimensional discrete convolution computed by means of 3 FFTs and by sampling either the non-paraxial (Rayleigh-Sommerfeld) or paraxial (Fresnel) propagation kernels. This method is developed in Section 2.2.

- **Propagation by the transfer function.** This method is similar to the propagation by convolution except that the propagation transfer function is directly sampled instead of being computed by the DFT of the sampled propagation kernel. Either the non-paraxial (Rayleigh-Sommerfeld) or the paraxial (Fresnel) propagation transfer functions may be used. This method costs 2 FFTs.

- **Propagation by the Fresnel transform.** Expanding the quadratic phase factor in the Fresnel propagation kernel in Eq. (58), the Fresnel diffraction integral may be rewritten as in Eq. (75) where the integral can be computed by a single Fourier transform. Hence, this method costs 1 FFT.

- **Propagation by the fractional Fourier transform.** This method, also called the 2-step Fresnel transform, amounts to performing two consecutive propagations by the Fresnel transform and hence costs 2 FFTs.

- **Fraunhofer propagation.** This method can be applied if the Fraunhofer conditions hold. For example, to propagate the field at a thin lens to the back focal plane of the lens. Fraunhofer propagation is done by a single FFT.

The computational cost is not the only thing to consider with these methods: there are also aliasing, sampling, and range issues. The convolution-based methods impose to keep the same sampling step in the input and output transverse planes, while the Fresnel transform imposes a magnification of the sampling step which depends on the propagation distance. In the 2-step Fresnel transform, there is some freedom for choosing the sampling step in the output transverse plane. Under the paraxial approximation, it is also possible to rewrite the convolution integral to have a sampling step in the output transverse plane that is not the same as in the input transverse plane. This latter method is exactly equivalent to a 2-step Fresnel transform.

According to Kopp and Meyrueis (1998), when the propagation is computed by a discrete convolution and FFTs, using the analytical expression or the propagation transfer function $\widetilde{h}_z(\boldsymbol{\alpha})$ rather that the FFT of the propagation kernel $h_z(\boldsymbol{x})$ is to be preferred: not only it is faster (by saving one two-dimensional FFT) but it also avoids aliasing (due to the fact that $\widetilde{h}_z(\boldsymbol{\alpha})$ is not band-limited).

[7] that is using FFTs for efficiency

2.1 Sampling

- Geometrical considerations give bounds on the frequencies. The unit-norm vector for the planar wave combination is $\boldsymbol{v} = \boldsymbol{k}/k = \left(v_x, v_y, \sqrt{1 - v_x^2 - v_y^2}\right)$ where $v_x = \sin\theta_x$ and $v_y = \sin\theta_y$ are the sine of the angles of $\boldsymbol{k}$ with the z–axis in the (x, z) and (y, z) longitudinal planes. It can be seen that, for any rays coming from the aperture at $z = 0$ and emerging from the aperture at z, the tangents of these angles are constrained by:

$$\tan\theta_x \in \left[\frac{x_{\max} - x'_{\min}}{z}, \frac{x_{\min} - x'_{\max}}{z}\right], \tag{78}$$

$$\tan\theta_y \in \left[\frac{y_{\max} - y'_{\min}}{z}, \frac{y_{\min} - y'_{\max}}{z}\right], \tag{79}$$

where $[x_{\min}, x_{\max}] \times [y_{\min}, y_{\max}]$ are the bounds of the aperture in the transverse plane at z while $[x'_{\min}, x'_{\max}] \times [y'_{\min}, y'_{\max}]$ are the bounds of the aperture in the transverse plane at $z = 0$. Since $\sin(\tan^{-1} t) = t/\sqrt{1 + t^2}$ (for the solution having the same sign as t), we have:

$$v_x = \sin\theta_x \in [p_z(x_{\max} - x'_{\min}), p_z(x_{\min} - x'_{\max})], \tag{80}$$

$$v_y = \sin\theta_y \in [p_z(y_{\max} - y'_{\min}), p_z(y_{\min} - y'_{\max})], \tag{81}$$

with:

$$p_z(x) = \frac{\operatorname{sign}(z)\, x}{\sqrt{z^2 + x^2}}. \tag{82}$$

Now, noting that the 2-dimensional frequency is $\boldsymbol{\alpha} = (v_x/\lambda, v_y/\lambda)$, the maximum amplitude of the frequency range is given by:

$$\begin{aligned}\Delta\alpha_{\max} = \max\big(&|p_z(x_{\max} - x'_{\min}) - p_z(x_{\min} - x'_{\max})|,\\ &|p_z(y_{\max} - y'_{\min}) - p_z(y_{\min} - y'_{\max})|\big)/\lambda\end{aligned} \tag{83}$$

can be computed for the considered setup. Accounting for periodic boundaries conditions[8], it is possible to completely avoid aliasing with the angular spectrum computed by an FFT provided that $\Delta\alpha_{\max} < N\,\delta\alpha$ with N the number of samples along a direction of the grid and $\delta\alpha$ the sampling step of the sampling frequencies. Hence the constraint can be expressed as $\delta x < \Delta\alpha_{\max}^{-1}$.

For centered apertures of diameters D and D', we have $x_{\min} = -D/2$, $x_{\max} = -D/2$, $x'_{\min} = -D'/2$, and $x'_{\max} = -D'/2$, and thus:

$$\delta x < \frac{\lambda}{2}\sqrt{1 + \left(z/\bar{D}\right)^2} \tag{84}$$

with $\bar{D} = (D + D')/2$ the mean diameter of the apertures. This condition reflects that, very near to the emitting aperture (for $z \ll \bar{D}$), oscillations of wavelength λ must be correctly sampled ($\lambda/2$ is the minimal sampling step for

[8] This means that the limitation is that the width of the interval must correspond to no more than N samples, not that the maximal (resp. minimal) position be at most $N/2$ (resp. at least $-N/2$) samples.

that). Very far from the emitting aperture, the condition becomes $\delta x/|z| < \frac{1}{2}\,\lambda/\bar{D}$ which amounts to correctly sampling the diffraction by an aperture of diameter $\bar{D}$.

In practice, the possible angles of emerging rays from the output aperture are not just set by geometrical rules but also by the diffraction which adds, say, a few λ/D radians to each end of the angular ranges, with D the largest size of the aperture.

For small aperture sizes compared to the propagation distance $|z|$, $p_z(x) \approx x/z$ and the constraint writes...

- For the 2-step Fresnel transform, geometrical considerations lead to the following constraint for the size of the domain to be sampled in the intermediate transverse plane at $z' = \beta\, z$:

$$L_{z'} \geq |1-\beta|\, L_0 + |\beta|\, L_z, \tag{85}$$

with L_0 and L_z the sizes of the apertures in the initial and final transverse planes. If the apertures are not isotropic, this condition applies for the two lateral dimensions. On the other hand, the FFTs in the 2 steps impose that:

$$N'\,\delta x_{z'}\,\delta x_0 = \lambda\,|z'| = \lambda\,|z|\,|\beta|, \tag{86}$$
$$N''\,\delta x_{z'}\,\delta x_z = \lambda\,|z''| = \lambda\,|z|\,|1-\beta|, \tag{87}$$

with δx_0, δx_z, $\delta x_{z'}$ the sampling steps in the transverse planes at positions 0, z, and z' along the longitudinal axis, and N' and N'' the number of samples per transverse axis used for the FFTs in the first and second steps (they are not ncessarily the same as we can use cropping and zero-padding provided there is no aliasing nor truncation). To avoid truncation and aliasing, the following conditions must hold:

$$N'\,\delta x_0 \geq L_0, \tag{88}$$
$$N'\,\delta x_{z'} \geq L_{z'}, \tag{89}$$
$$N''\,\delta x_z \geq L_z, \tag{90}$$
$$N''\,\delta x_{z'} \geq L_{z'}. \tag{91}$$

Combining Eqs. (85), (86), and (89) yields:

$$N'\,\delta x_{z'} = \lambda\,|z|\,|\beta|/\delta x_0 \geq |1-\beta|\, L_0 + |\beta|\, L_z \tag{92}$$

Unless $L_0 = 0$, β must be non-zero for the above inequality to hold, and thus we can divide the two last right-hand sides by $|\beta|$ to obtain:

$$\lambda\,|z|/\delta x_0 \geq |1-1/\beta|\, L_0 + L_z. \tag{93}$$

In particular, this shows that:

$$\boxed{\delta x_0 \leq \lambda\,|z|/L_z} \tag{94}$$

must hold. Similarly, combining Eqs. (85), (87), and (91) yields:

$$N'' \, \delta x_{z'} = \lambda \, |z| \, |1 - \beta| / \delta x_z \geq |1 - \beta| \, L_0 + |\beta| \, L_z \tag{95}$$

Unless $L_z = 0$, β must be different from one for the above inequality to hold, and thus we can divide the two last right-hand sides by $|1 - \beta|$ to obtain:

$$\lambda \, |z| / \delta x_z \geq L_0 + |1 - 1/\beta|^{-1} \, L_z. \tag{96}$$

In particular, this shows that:

$$\boxed{\delta x_z \leq \lambda \, |z| / L_0} \tag{97}$$

must hold. Even though the Fresnel transform assumes paraxial conditions, that is $|z| \gg L_0$ and $|z| \gg L_z$, conditions in Eqs. (94) and (98) impose conditions on the smalness of the sampling steps for the considered propagation. These conditions can be summarized by the following condition that must hold for the sampling step δx_j of any transverse plane of a numerical simulation:

$$\delta x_j \leq \min_{j' \in \mathbb{S}_j} \lambda_{j,j'} \, |z_{j'} - z_j| / L_{j'} \tag{98}$$

where $\mathbb{S}_j$ is the set of other transverse planes from which the j-th plane directly receives a wave or to which the j-th plane directly emits a wave, $\lambda_{j,j'}$ is the wavelength of the medium between the j-th and j'-th transverse planes, $z_{j'}$ and $L_{j'}$ are respectively the position along the longitudinal axis the transverse size of the aperture in the j'-th transverse plane.

Assuming these conditions hold, then:

$$\frac{L_z}{\lambda \, |z| / \delta x_z - L_0} \leq |1 - 1/\beta| \leq \frac{\lambda \, |z| / \delta x_0 - L_z}{L_0} \tag{99}$$

Not that the extreme hand sides impose an additional constraint on the smallness of the sampling steps.

For numerical computations, the continuous functions of the transverse position and spatial frequency are sampled on a regular Cartesian grid. We further assume that the number of samples and the sampling steps are the same along the 2 transverse dimensions. In other words, we use $N \times N$ grids of equally spaced nodes. This subsection briefly introduces the relations between the sampled field and the sampled angular spectrum based on the properties developed in Appendix C.

Following our assumptions, the transverse plane is considered to be sampled on a $N \times N$ grid with step δx at positions:

$$\boldsymbol{x}[\boldsymbol{j}] = \delta x \times \boldsymbol{j} \tag{100}$$

for all $\boldsymbol{j} \in \mathbb{J}^2$ and where (following FFT conventions):

$$\mathbb{J} = \begin{cases} [\![-\frac{N}{2}, \frac{N}{2} - 1]\!] & \text{if } N \text{ even} \\ [\![-\frac{N-1}{2}, \frac{N-1}{2}]\!] & \text{if } N \text{ odd.} \end{cases} \tag{101}$$

To simplify the notation and avoid ambiguities, we use square brackets to indicate sampling, bold-face lower-case letters for vectors (indexed collections of values), and bold-face upper-case letters for linear operators (matrices). For example, $u_z(\boldsymbol{x})$ is the field in the transverse plane at longitudinal position z and transverse position $\boldsymbol{x}$, while $u_z[\boldsymbol{j}] \equiv u_z(\boldsymbol{x}[\boldsymbol{j}])$ is the sampled field at grid index $\boldsymbol{j}$. As another example, $u_z{:}\mathbb{R}^2 \to \mathbb{C}$ is the field as a continuous function of the transverse position, while $\boldsymbol{u}_z \in \mathbb{C}^{N^2}$ is the sampled field, that is the vector whose entries are $u_z[\boldsymbol{j}]$ for all $\boldsymbol{j} \in \mathbb{J}^2$.

The **sampled angular spectrum** at frequency $\boldsymbol{\alpha}[\boldsymbol{j}] = \delta\alpha \times \boldsymbol{j}$ can be computed by using a Riemman sum approximation of the continuous Fourier transform integral:

$$\begin{aligned} \widetilde{u}_z[\boldsymbol{j}] = \widetilde{u}_z(\boldsymbol{\alpha}[\boldsymbol{j}]) &= \iint \mathrm{e}^{-\mathrm{i}\,2\,\pi\,\langle \boldsymbol{\alpha}[\boldsymbol{j}], \boldsymbol{x}\rangle}\, u_z(\boldsymbol{x})\,\mathrm{d}\boldsymbol{x} \\ &\approx \delta x^2 \sum_{\boldsymbol{j}' \in \mathbb{J}^2} \underbrace{\mathrm{e}^{-\mathrm{i}\,2\,\pi\,\langle \boldsymbol{\alpha}[\boldsymbol{j}], \boldsymbol{x}[\boldsymbol{j}']\rangle}}_{F_{\boldsymbol{j},\boldsymbol{j}'}} \underbrace{u_z(\boldsymbol{x}[\boldsymbol{j}'])}_{u_z[\boldsymbol{j}']} \end{aligned} \tag{102}$$

which, using linear algebra notation, yields the following numerical approximations for the sampled field and angular spectrum:

$$\widetilde{\boldsymbol{u}}_z = \delta x^2\, \mathbf{F} \cdot \boldsymbol{u}_z \tag{103}$$

$$\boldsymbol{u}_z = \delta\alpha^2\, \mathbf{F}^\star \cdot \widetilde{\boldsymbol{u}}_z \tag{104}$$

where $\mathbf{F}$ is the *discrete Fourier transform* (DFT) operator whose entries are given by:

$$F_{\boldsymbol{j},\boldsymbol{j}'} = \mathrm{e}^{-\mathrm{i}\,2\,\pi\,\langle \boldsymbol{\alpha}_{\boldsymbol{j}}, \boldsymbol{x}_{\boldsymbol{j}'}\rangle} = \mathrm{e}^{-\mathrm{i}\,2\,\pi\,\delta x\,\delta\alpha\,\langle \boldsymbol{j},\boldsymbol{j}'\rangle} \tag{105}$$

where $\langle \boldsymbol{a}, \boldsymbol{b}\rangle$ denotes the inner (or scalar) product of the vectors $\boldsymbol{a}$ and $\boldsymbol{b}$. The $N \times N$ DFT can be computed by the *fast Fourier transform* (FFT) in $\mathcal{O}(N^2\,\log_2 N)$ operations. As shown by Eqs. (231) and (235) in Appendix C, having $\mathbf{F}$ inversible imposes:

$$N\,\delta x\,\delta\alpha = 1, \tag{106}$$

and thus:

$$F_{\boldsymbol{j},\boldsymbol{j}'} = \mathrm{e}^{-\mathrm{i}\,2\,\pi\,\langle \boldsymbol{j},\boldsymbol{j}'\rangle/N}, \tag{107}$$

and:

$$\left(\delta x^2\,\mathbf{F}\right) \cdot \left(\delta\alpha^2\,\mathbf{F}^\star\right) = N^{-2}\,\mathbf{F} \cdot \mathbf{F}^\star = \mathbf{I}, \tag{108}$$

with $\mathbf{I}$ the matrix identity of suitable size.

2.2 Propagation by convolution

As stated by Eq. (26), propagation of the field $u_0(\boldsymbol{x})$ in the input transverse plane at $z = 0$ to the transverse plane at z can be expressed as a convolution:

$$u_z(\boldsymbol{x}) = \iint h_z(\boldsymbol{x} - \boldsymbol{x}')\, u_0(\boldsymbol{x}')\,\mathrm{d}\boldsymbol{x}' \tag{109}$$

with $h_z(\boldsymbol{x})$ the propagation kernel. For the Rayleigh-Sommerfeld diffraction integral, in Eq. (49), the propagation kernel is given in Eq. (51). For Fresnel diffraction, that is in paraxial conditions, the propagation kernel is given in Eq. (58).

This type of propagation can be numerically approximated by a discrete convolution:

$$u_z[\boldsymbol{j}] = u_z(\boldsymbol{x}[\boldsymbol{j}]) \approx \sum_{\boldsymbol{j}'} h_z[\boldsymbol{j} - \boldsymbol{j}']\, u_0[\boldsymbol{j}']\, \delta x^2 \tag{110}$$

where $h_z[\boldsymbol{j} - \boldsymbol{j}'] = h_z(\delta x\,(\boldsymbol{j} - \boldsymbol{j}')) = h_z(\boldsymbol{x}[\boldsymbol{j}] - \boldsymbol{x}[\boldsymbol{j}'])$ and $u_0[\boldsymbol{j}] = u_0(\boldsymbol{x}[\boldsymbol{j}'])$ are the sampled propagation kernel and input field. The discrete convolution can be quickly computed by 3 FFTs. Give the expression in algebra notation.

There are however 2 issues to take care of:

1. To avoid aliasing, the size of the sampled area must be sufficiently large (using zero padding to extend the supports of the beam in the input and output transverse planes).

2. To provide a good approximation, the variations of all the functions involved in the convolution (the input field and the kernel) must be correctly sampled which imposes a lower bound on the sampling step δx or an upper bound of the propagation range z.

These issues are discussed next.

2.2.1 Support constraint in propagation by convolution

To limit the number of operations, the sum in the discrete convolution in Eq. (110) shall only be performed for $\boldsymbol{x}[\boldsymbol{j}'] \in \Omega_0$ where Ω_0 includes the transverse positions where the field u_0 in the input transverse plane is non-zero. At least:

$$u_0[\boldsymbol{j}'] \neq 0 \quad \Longrightarrow \quad \boldsymbol{x}[\boldsymbol{j}'] \in \Omega_0. \tag{111}$$

The discrete convolution shall also only be computed for nodes $\boldsymbol{j}$ where the field in the output transverse plane is non-zero. Due to diffraction, it is not possible to strictly impose such a restriction but we may assume that a mask is placed in the output transverse plane so that we can define Ω_z which includes the transverse positions where the field in the output transverse plane is non-zero *after* the mask. Said otherwise, we assume that we are only interested in having the field in the output transverse plane for a limited support Ω_z. For practical reasons and since we are interested in making as few operations as possible, the supports Ω_0 and Ω_z must have finite sizes and shall be as small as possible.

For a faster computation of the discrete convolution, the discrete Fourier transform (DFT) may be used, but to avoid aliasing, the size of the grid must be large enough. Denoting L_0 and L_z the maximum number of samples along any dimension of Ω_0 and Ω_z, the minimal size of the support of the propagation kernel is $L = L_0 + L_z - 1$ to account for all possible values of $\boldsymbol{j} - \boldsymbol{j}'$ and the (unwrapped) output discrete convolution has size $L + L_0 - 1$. Finally, to avoid aliasing, the minimal grid size is:

$$N \geq L_0 + L_z - 1. \tag{112}$$

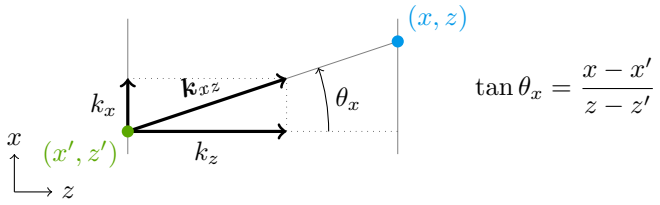

Figure 3: Plane wave from a point (in green) of the input transverse plane to a point (in blue) of the output transverse plane. $\boldsymbol{k}_{xz}$ is the wave-vector projected in the (x, z) plane, while k_x and k_z are the Cartesian coordinates of the wave-vector along the x and z axes.

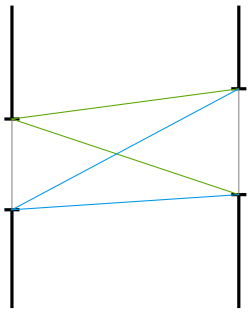

Figure 4: Propagation between two apertures.

If the supports, Ω_0, Ω_z, and $\Omega = \Omega_z - \Omega_0$ are not centered, the output angular spectrum may be multiplied by a linear phase factor before applying the inverse DFT. (Not clear and supports are assumed centered in the 2 next subsections.)

The corresponding angular frequency is $\alpha_x = k_x/(2\,\pi) = \sin(\theta_x)/\lambda$.

$$\boldsymbol{\alpha} = \frac{(k_x, k_y)}{2\,\pi} = \frac{(\sin\theta_x, \sin\theta_y)}{\lambda} = \frac{(x - x', y - y')}{\lambda\,\Delta r} = \frac{\boldsymbol{x} - \boldsymbol{x}'}{\lambda\,\sqrt{\|\boldsymbol{x} - \boldsymbol{x}'\|^2 + (z - z')^2}} \tag{113}$$

with $\Delta r = \sqrt{(x - x')^2 + (y - y')^2 + (z - z')^2}$

In the considered conditions and assuming square supports to simplify, the direct computation of the discrete convolution by Eq. (110) takes about $2\,L_0^2\,L_z^2 \sim 2\,L^4$ operations with L the typical value of L_0 and L_z. Computation by fast Fourier transform (FFT) takes about $3\,N^2\,\log_2 N^2 \sim 3\,(3\,L)^2\,\log_2((3\,L)^2) \sim 54\,L^2\,\log_2 L$ operations. For large[9] L's, the FFT-based method is much faster despite the larger size of the required grid.

[9] not so large in fact, since the FFT-based method is faster for $L \geq 10$ ignoring overheads

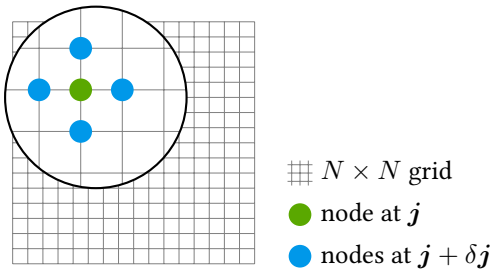

Figure 5: Closest nodes on a grid. In green, the considered node at index $\delta\boldsymbol{j}$; in blue, its closest neighbors at index $\delta\boldsymbol{j} + \delta\boldsymbol{j}$ with $\delta\boldsymbol{j} \in \{(\pm 1, 0), (0, \pm 1)\}$.

2.2.2 Sampling and range constraints in Rayleigh-Sommerfeld diffraction

The propagation kernel $h_z(\boldsymbol{x})$ in Rayleigh-Sommerfeld diffraction is given by Eq. (51) and the most constraining term for the sampling step is the phase of the $\mathrm{e}^{\mathrm{i}\,k\,r}$ term since it varies by more than π radians when the variation of r between adjacent samples is greater than $\lambda/2$.

In Rayleigh-Sommerfeld kernel $h_z(\boldsymbol{x})$ given by Eq. (51), the propagation distance is:

$$r(\boldsymbol{x}) = \sqrt{\|\boldsymbol{x}\|^2 + z^2} \tag{114}$$

with $z > 0$ the distance along the optical axis between the input and output transverse planes. To avoid irreversible phase wrapping, the phase difference between two adjacent nodes of the sampling grid must not be greater than π which yields the condition $k\,\delta r_{\max} \leq \pi$ or equivalently $\delta r_{\max} \leq \lambda/2$ with $\delta r_{\max}$ the greatest absolute variation of r between 2 adjacent nodes in the sampling grid:

$$\delta r_{\max} = \max_{\substack{\boldsymbol{x}\in\Omega \\ \delta\boldsymbol{x}\in\delta\Omega}} |r(\boldsymbol{x} + \delta\boldsymbol{x}) - r(\boldsymbol{x})| \tag{115}$$

with $\Omega = \Omega_z - \Omega_0$ the discrete kernel support accounting for all differences in transverse positions between the input and output transverse planes and:

$$\delta\Omega = \{(\pm\delta x, 0), (0, \pm\delta x)\} \tag{116}$$

the offsets to the closest sampled nodes (the blue dots in Fig. 5).

Since it is required that δx be small enough to correctly sample the variations of r, the following approximation can be made:

$$r(\boldsymbol{x} + \delta\boldsymbol{x}) - r(\boldsymbol{x}) \approx \left\langle \frac{\partial r(\boldsymbol{x})}{\partial \boldsymbol{x}}, \delta\boldsymbol{x} \right\rangle = \frac{\langle \boldsymbol{x}, \delta\boldsymbol{x} \rangle}{r(\boldsymbol{x})} \tag{117}$$

where $\langle , \rangle$ denotes the inner (scalar) product. Hence:

$$\delta r_{\max} \approx \max_{\substack{\boldsymbol{x}\in\Omega \\ \delta\boldsymbol{x}\in\delta\Omega}} \left| \frac{\langle \boldsymbol{x}, \delta\boldsymbol{x} \rangle}{r(\boldsymbol{x})} \right| = \max_{\boldsymbol{x}\in\Omega} \frac{\max_{\delta\boldsymbol{x}\in\delta\Omega} |\langle \boldsymbol{x}, \delta\boldsymbol{x} \rangle|}{r(\boldsymbol{x})} \tag{118}$$

From the definition of $\delta\Omega$ in Eq. (116), the numerator in the last above right-hand side can be simplified to:

$$\max_{\delta\boldsymbol{x}\in\delta\Omega} |\langle \boldsymbol{x}, \delta\boldsymbol{x}\rangle| = \delta x \, \|\boldsymbol{x}\|_\infty \tag{119}$$

with $\|\boldsymbol{x}\|_\infty = \max(|x|, |y|)$ the infinite norm of $\boldsymbol{x} = (x, y)$ and then:

$$\delta r_{\max} \approx \delta x \max_{\boldsymbol{x}\in\Omega} \frac{\|\boldsymbol{x}\|_\infty}{r(\boldsymbol{x})}. \tag{120}$$

Clearly, the nodes that have a given $\|\boldsymbol{x}\|_\infty = \ell$ and yet the least $r(\boldsymbol{x})$ are those such that $\boldsymbol{x} = (\pm\ell, 0)$ or $\boldsymbol{x} = (0, \pm\ell)$, hence:

$$\delta r_{\max} \approx \delta x \max_{\boldsymbol{x}\in\Omega} \frac{\|\boldsymbol{x}\|_\infty}{\sqrt{\|\boldsymbol{x}\|_\infty^2 + z^2}}. \tag{121}$$

Deriving the function:

$$\delta r(\ell) = \frac{\ell}{\sqrt{\ell^2 + z^2}} \tag{122}$$

yields:

$$\delta r'(\ell) = \frac{z^2}{(\ell^2 + z^2)^{3/2}} \tag{123}$$

which is non-negative, hence $\delta r(\ell)$ is increasing with ℓ. The maximal value for δr is thus found at $\ell_{\max} = \max_{\boldsymbol{x}\in\Omega} \|\boldsymbol{x}\|_\infty = D/2$ with D the transverse size of Ω and finally:

$$\delta r_{\max} \approx \frac{\delta x \, D/2}{\sqrt{z^2 + (D/2)^2}} = \frac{\delta x/2}{\sqrt{(z/D)^2 + 1/4}}. \tag{124}$$

The sampling condition for the Rayleigh-Sommerfeld kernel, that is $\delta r_{\max} \leq \lambda/2$, finally writes:

$$\frac{\delta x}{\sqrt{(z/D)^2 + 1/4}} \leq \lambda. \tag{125}$$

This condition may be expressed as an upper bound on the sampling step:

$$\delta x \leq \delta x_{\max} = \lambda \sqrt{(z/D)^2 + 1/4} \approx \begin{cases} \lambda/2 & \text{when } |z| \ll D \\ |z| \, \lambda/D & \text{when } |z| \gg D \end{cases} \tag{126}$$

with D the transverse size of Ω. In the near field, that is for $z \ll D$, the bound is the Shannon sampling step to correctly sample all propagating waves which have spatial frequencies up to $1/\lambda$. In the far field, that is for $z \gg D$, the bound is the propagation distance along the optical axis times the angular diffraction limit λ/D for an aperture of size D. Note that, even though the angular spectrum $\widetilde{u}_0(\boldsymbol{\alpha})$ of the field in the input transverse plane has a cutoff frequency much smaller than $1/(2\,\delta x_{\max})$, the constraint $\delta x \leq \delta x_{\max}$ still applies to avoid undersampling the kernel before computing its discrete Fourier transform. To benefit from a cutoff frequency of the angular spectrum, another method must be considered where the propagation transfer function $\widetilde{h}_z(\boldsymbol{\alpha})$ is directly sampled.

Looking at Eq. (126), it is clear that having the smallest possible D is desirable to relax the constraint on the smallness of the sampling step. Going back to the discussion about the sizes of the supports, near Eq. (112), it can be seen that the smallest possible support size to sample the propagation kernel is $D = D_0 + D_z$ where $D_0 = L_0\,\delta x$ and $D_z = L_z\,\delta x$ are the respective sizes of the supports of the field in the input and output transverse planes.

For a chosen sampling step, the sampling condition in Eq. (126) can be converted into a minimal range condition to apply this propagation method:

$$|z| \geq D\,\sqrt{(\delta x/\lambda)^2 - 1/4} \tag{127}$$

provided $\delta x > \lambda/2$; otherwise, $|z|$ can be as small as a few wavelengths[10]. Again, to relax as much as possible this constraint, D must be as small as possible.

Remember that Rayleigh-Sommerfeld diffraction integral assumes $z \geq 0$, that is forward propagation, **reverse propagation** can nevertheless be implemented as the deconvolution by the forward propagation kernel. Give the formal expression.

2.2.3 Sampling and range constraints for paraxial propagation kernel

The paraxial (Fresnel) propagation kernel is given by Eq. (58) which we recall for convenience:

$$h_z(\boldsymbol{x}) = \frac{\mathrm{e}^{\mathrm{i}\,k\,z}}{\mathrm{i}\,\lambda\,z}\,\mathrm{e}^{\mathrm{i}\,\pi\,\|\boldsymbol{x}\|^2/(\lambda\,z)}. \tag{128}$$

Now the phase is varying as $\phi(\boldsymbol{x}) = \pi\,\|\boldsymbol{x}\|^2/(\lambda\,z)$ a quadratic function of the transverse position $\boldsymbol{x}$. The maximal absolute difference of the quadratic phase between adjacent nodes of the grid is:

$$\delta\phi_{\max} = \max_{\substack{\boldsymbol{x}\in\Omega\\ \delta\boldsymbol{x}\in\delta\Omega}} |\phi(\boldsymbol{x}+\delta\boldsymbol{x}) - \phi(\boldsymbol{x})| \tag{129}$$

$$= \frac{\pi}{\lambda\,|z|} \max_{\substack{\boldsymbol{x}\in\Omega\\ \delta\boldsymbol{x}\in\delta\Omega}} \left| \|\boldsymbol{x}+\delta\boldsymbol{x}\|^2 - \|\boldsymbol{x}\|^2 \right| \tag{130}$$

with, as in the previous subsection, $\Omega = \Omega_0 - \Omega_z$ the set of nodes for which the kernel must be evaluated and $\delta\Omega$ given in Eq. (116) the offsets to the adjacent nodes. To estimate $\delta\phi_{\max}$, we compute:

$$\max_{\substack{\boldsymbol{x}\in\Omega\\ \delta\boldsymbol{x}\in\delta\Omega}} \left| \|\boldsymbol{x}+\delta\boldsymbol{x}\|^2 - \|\boldsymbol{x}\|^2 \right| = \max_{\substack{\boldsymbol{x}\in\Omega\\ \delta\boldsymbol{x}\in\delta\Omega}} \left| \|\delta\boldsymbol{x}\|^2 + 2\,\langle \boldsymbol{x}, \delta\boldsymbol{x}\rangle \right| \tag{131}$$

$$= \max_{\substack{\boldsymbol{x}\in\Omega\\ \delta\boldsymbol{x}\in\delta\Omega}} \left| \delta x^2 + 2\,\langle \boldsymbol{x}, \delta\boldsymbol{x}\rangle \right| \tag{132}$$

$$= \delta x^2 + 2 \max_{\substack{\boldsymbol{x}\in\Omega\\ \delta\boldsymbol{x}\in\delta\Omega}} |\langle \boldsymbol{x}, \delta\boldsymbol{x}\rangle| \tag{133}$$

$$= \delta x^2 + 2\,\delta x \max_{\boldsymbol{x}\in\Omega} \|\boldsymbol{x}\|_\infty \tag{134}$$

$$= \delta x^2 + \delta x\,D \tag{135}$$

[10] if $|z|$ is less than a few λ, evanescent waves must be taken into account

where right-hand side (132) follows from $\|\delta\boldsymbol{x}\| = \delta x$ for any $\delta\boldsymbol{x} \in \delta\Omega$ with $\delta\Omega$ defined in Eq. (116), right-hand side (134) follows from Eq. (119), and right-hand side (135) follows from $\max_{\boldsymbol{x}\in\Omega}\|\boldsymbol{x}\|_\infty = D/2$ with D the transverse size of Ω. Note that, contrarily to the computations in Eq. (117), there are no approximations here. The maximal absolute difference of the quadratic phase

$$\delta\phi_{\max} = \max_{\substack{\boldsymbol{x}\in\Omega \\ \delta\boldsymbol{x}\in\delta\Omega}} |\phi(\boldsymbol{x}+\delta\boldsymbol{x}) - \phi(\boldsymbol{x})| = \frac{\pi\,(D+\delta x)\,\delta x}{\lambda\,|z|} \approx \frac{\pi\,D\,\delta x}{\lambda\,|z|}, \tag{136}$$

the latter approximation since $D \gg \delta x$ in general. The condition $\delta\phi_{\max} \leq \pi$ amounts to:

$$\frac{D\,\delta x}{\lambda\,|z|} \leq 1 \tag{137}$$

which may be seen as an upper bound for the sampling step:

$$\delta x \leq |z|\,\lambda/D, \tag{138}$$

or as a minimal propagation range condition:

$$|z| \geq D\,\delta x/\lambda. \tag{139}$$

Compared to Eq. (126), Eq. (138) corresponds to the far field case $|z| \gg D$; while, compared to Eq. (127), Eq. (139) corresponds to $\delta x \gg \lambda/2$.

Note that the paraxial approximation of the propagation kernel assumes that the condition in Eq. (73) holds which is equivalent to:

$$|z| \gg \left(\frac{\|\boldsymbol{x}\|^4}{8\,\lambda}\right)^{1/3} \tag{140}$$

although Southwell (1981) has shown that, in practice, the Fresnel approximation works quite well for propagation distances much smaller than that.

2.3 Angular spectrum propagation

The angular spectrum propagation method is similar to the propagation by convolution computed by means of FFT's, the only difference is that the propagation transfer function $\widetilde{h}_z(\boldsymbol{\alpha})$ is directly sampled instead of being given by a DFT of the sampled propagation kernel $h_z(\boldsymbol{x})$. This numerical approximation of the optical propagation writes:

$$\begin{aligned}\boldsymbol{u}_z &= \left(\delta\alpha^2\,\mathbf{F}^\star\right)\cdot\mathrm{diag}\left(\widetilde{\boldsymbol{h}}_z\right)\cdot\left(\delta x^2\,\mathbf{F}\right)\cdot\boldsymbol{u}_0 \\ &= \underbrace{\frac{1}{N^2}\cdot\mathbf{F}^\star\cdot\mathrm{diag}\left(\widetilde{\boldsymbol{h}}_z\right)\cdot\mathbf{F}}_{\text{propagator}}\cdot\boldsymbol{u}_0\end{aligned} \tag{141}$$

since $\delta x\,\delta\alpha = 1/N$ for the approximation of the Fourier transform by the DFT operator $\mathbf{F}$ and with $\mathrm{diag}(\widetilde{\boldsymbol{h}}_z)$ the linear operator implementing element-wise multiplication by $\widetilde{\boldsymbol{h}}_z$ the propagation transfer function sampled at discrete frequencies $\boldsymbol{\alpha}[\boldsymbol{j}] = \delta\alpha\,\boldsymbol{j}$.

The first condition that must hold to apply this method is that the Nyquist frequency for a $N \times N$ grid of discrete spatial frequencies:

$$\alpha_{\text{samp}} = (N/2)\,\delta\alpha = \frac{1}{2\,\delta x} \tag{142}$$

must not be smaller than the cutoff frequency α_{cut} of the input angular spectrum:

$$\alpha_{\text{samp}} \geq \alpha_{\text{cut}} \quad \Longrightarrow \quad \delta x \leq \frac{1}{2\,\alpha_{\text{cut}}} \tag{143}$$

Note that, taking the intensity, that is the squared modulus of the complex amplitude, effectively doubles the cutoff frequency.

As before but in the frequency space, another condition to approximate the integral over frequencies for the final Fourier transform by a Riemann sum is that the frequency sampling step $\delta\alpha$ be fine enough to correctly sample the variation of the propagation transfer function $\widetilde{h}_z(\boldsymbol{\alpha})$. This depends on the considered case, non-paraxial or paraxial as examined next.

2.4 Angular spectrum frequencies

The diffraction integral states that, when propagating from $\boldsymbol{r}' \in \Sigma$ to $\boldsymbol{r}$, the phase of the field becomes:

$$\phi(\boldsymbol{r}, \boldsymbol{r}') = \varphi_{z'}(\boldsymbol{x}') + \psi(\boldsymbol{r}, \boldsymbol{r}') \tag{144}$$

where $\varphi_{z'}(\boldsymbol{x}')$ is the phase of the wavefront leaving the input transverse plane at z' while $\psi_{z-z'}(\boldsymbol{x} - \boldsymbol{x}') = \arg(h_{z-z'}(\boldsymbol{x} - \boldsymbol{x}'))$ is the phase shift due to the propagation kernel. The phase $\varphi_{z'}(\boldsymbol{x}')$ is introduced for generality, it may account for the phase of the complex amplitude transmission of the aperture in the input transverse plane, for a quadratic phase term due to a thin lens or to the Fresnel transform in the paraxial conditions, etc.

The variation of the phase $\phi(\boldsymbol{r}, \boldsymbol{r}')$ in the input transverse plane can be interpreted as the transverse wave-vector $\boldsymbol{k}_\perp$ of a planar wave propagating from $\boldsymbol{r}'$ to $\boldsymbol{r}$:

$$\boldsymbol{k}_\perp(\boldsymbol{r}, \boldsymbol{r}') = \frac{\partial\phi(\boldsymbol{r}, \boldsymbol{r}')}{\partial\boldsymbol{x}'} \tag{145}$$

which corresponds, see Eq. (47), to the angular spectrum frequency:

$$\boldsymbol{\alpha}(\boldsymbol{r}, \boldsymbol{r}') = \frac{\boldsymbol{k}_\perp(\boldsymbol{r}, \boldsymbol{r}')}{2\,\pi} = \frac{1}{2\,\pi}\,\frac{\partial\phi(\boldsymbol{r}, \boldsymbol{r}')}{\partial\boldsymbol{x}'}. \tag{146}$$

Now if the field $u_{z'}(\boldsymbol{x}')$ in the input transverse plane at z' has a finite size support[11] $\Omega' \subset \Sigma$ and if we only need to estimate the field $u_z(\boldsymbol{x})$ over a finite size subset, Ω, of the output transverse plane at z, the angular spectrum propagation can be restricted to the frequencies $\boldsymbol{\alpha} \in \Xi$ with Ξ the set of propagating frequencies defined by:

$$\Xi = \{\boldsymbol{\alpha}(\boldsymbol{r}, \boldsymbol{r}') \,|\, \boldsymbol{r} \in \Omega \text{ and } \boldsymbol{r}' \in \Omega'\} \tag{147}$$

[11] The support of a function contains all arguments where the function is non-zero.

where $\boldsymbol{\alpha}(\boldsymbol{r}, \boldsymbol{r}')$ is defined in Eq. (146). Note that Ξ is finite following from Ω' and Ω' being both finite. Having a finite range of frequencies to consider is crucial to limit the numerical complexity of performing the propagation by the angular spectrum method.

2.4.1 Propagation by the non-paraxial transfer function

The non-paraxial transfer function given in Eq. (44) is:

$$\widetilde{h}_z(\boldsymbol{\alpha}) = \mathrm{e}^{\mathrm{i}\,k\,z\,\sqrt{1-\|\lambda\,\boldsymbol{\alpha}\|^2}}. \tag{148}$$

Evanescent waves whose frequencies are greater than $1/\lambda$ are rapidly vanishing and negligible for $|z|$ greater or equal a few wavelengths. Hence, we shall only consider propagating waves, that is spatial frequencies such that $\|\boldsymbol{\alpha}\| < 1/\lambda$. For these frequencies, the variations of the phase

$$\phi(\boldsymbol{\alpha}) = k\,z\,\sqrt{1-\|\lambda\,\boldsymbol{\alpha}\|^2} \tag{149}$$

of the transfer function between contiguous discrete frequencies must not be greater than π which imposes that:

$$|\phi(\boldsymbol{\alpha}+\delta\boldsymbol{\alpha}) - \phi(\boldsymbol{\alpha})| \leq \pi \tag{150}$$

must hold for any $\boldsymbol{\alpha} \in \Xi$ and any $\delta\boldsymbol{\alpha} \in \delta\Xi$ with:

$$\delta\Xi = \{(\pm\delta\alpha, 0), (0, \pm\delta\alpha)\} \tag{151}$$

the offsets to contiguous spatial frequencies (the blue dots in Fig. 5) and with:

$$\Xi = \left\{\boldsymbol{\alpha} \in \mathbb{R}^2 \,\middle|\, \|\boldsymbol{\alpha}\|_\infty \leq \alpha_{\mathrm{samp}} \text{ and } \|\boldsymbol{\alpha}\| < \min(\alpha_{\mathrm{cut}}, 1/\lambda)\right\} \tag{152}$$

the domain of spatial frequencies to consider with α_{samp} the Nyquist frequency defined in Eq. (142) and $\min(\alpha_{\mathrm{cut}}, 1/\lambda)$ the maximal frequency of waves existing in the input angular spectrum and that can propagate.

Assuming the spectral sampling step $\delta\alpha = 1/(N\,\delta x)$ is small enough, the maximal absolute phase difference can be estimated following the same steps as in section 2.2.2:

$$\begin{aligned}
\delta\phi_{\max} &= \max_{\substack{\boldsymbol{\alpha}\in\Xi \\ \delta\boldsymbol{\alpha}\in\delta\Xi}} |\phi(\boldsymbol{\alpha}+\delta\boldsymbol{\alpha}) - \phi(\boldsymbol{\alpha})| && (153)\\
&\simeq \max_{\substack{\boldsymbol{\alpha}\in\Xi \\ \delta\boldsymbol{\alpha}\in\delta\Xi}} \left|\left\langle \frac{\partial\phi(\boldsymbol{\alpha})}{\partial\boldsymbol{\alpha}}, \delta\boldsymbol{\alpha}\right\rangle\right| && (154)\\
&= 2\,\pi\,|z|\,\lambda \max_{\substack{\boldsymbol{\alpha}\in\Xi \\ \delta\boldsymbol{\alpha}\in\delta\Xi}} \left|\frac{\langle\boldsymbol{\alpha}, \delta\boldsymbol{\alpha}\rangle}{\sqrt{1-\|\lambda\,\boldsymbol{\alpha}\|^2}}\right| && (155)\\
&= 2\,\pi\,|z|\,\lambda \max_{\boldsymbol{\alpha}\in\Xi} \frac{\max_{\delta\boldsymbol{\alpha}\in\delta\Xi}|\langle\boldsymbol{\alpha}, \delta\boldsymbol{\alpha}\rangle|}{\left|\sqrt{1-\|\lambda\,\boldsymbol{\alpha}\|^2}\right|} && (156)\\
&= 2\,\pi\,|z|\,\lambda\,\delta\alpha \max_{\boldsymbol{\alpha}\in\Xi} \frac{\|\boldsymbol{\alpha}\|_\infty}{\left|\sqrt{1-\|\lambda\,\boldsymbol{\alpha}\|^2}\right|}. && (157)
\end{aligned}$$

If $\max_{\boldsymbol{\alpha}\in\Xi}\|\boldsymbol{\alpha}\| = \min(\alpha_{\text{cut}}, \sqrt{2}\,\alpha_{\text{samp}}) \geq 1/\lambda$, then $\sqrt{1-\|\lambda\,\boldsymbol{\alpha}\|^2}$ may be arbitrarily close to zero for $\|\boldsymbol{\alpha}\|_\infty > 0$. Hence, the condition in Eq. (150) cannot hold and phase wrapping is irreversible. Otherwise, maximizing the right-hand-side in Eq. (157) amounts to finding the frequencies in Ξ such that $\|\boldsymbol{\alpha}\|_\infty$ and $\|\boldsymbol{\alpha}\|$ are both maximized. The 3 possibilities are illustrated by Fig. 6. If $\sqrt{2}\,\alpha_{\text{samp}} < \min(1/\lambda, \alpha_{\text{cut}})$, then the worst spatial frequencies are indicated by blue dots in the leftmost panel of Fig. 6 and:

$$\max_{\boldsymbol{\alpha}\in\Xi} \frac{\|\boldsymbol{\alpha}\|_\infty}{\left|\sqrt{1-\|\lambda\,\boldsymbol{\alpha}\|^2}\right|} = \frac{\alpha_{\text{samp}}}{\sqrt{1-2\,\lambda^2\,\alpha_{\text{samp}}^2}}; \tag{158}$$

else if $\alpha_{\text{samp}} \leq \alpha_{\text{cut}} < 1/\lambda$, then the worst spatial frequencies are indicated by green dots in the central panel of Fig. 6 and:

$$\max_{\boldsymbol{\alpha}\in\Xi} \frac{\|\boldsymbol{\alpha}\|_\infty}{\left|\sqrt{1-\|\lambda\,\boldsymbol{\alpha}\|^2}\right|} = \frac{\alpha_{\text{samp}}}{\sqrt{1-\lambda^2\,\alpha_{\text{cut}}^2}}; \tag{159}$$

finally, if $\alpha_{\text{cut}} < \min(1/\lambda, \alpha_{\text{samp}})$, then the worst spatial frequencies are indicated by orange dots in the rightmost panel of Fig. 6 and:

$$\max_{\boldsymbol{\alpha}\in\Xi} \frac{\|\boldsymbol{\alpha}\|_\infty}{\left|\sqrt{1-\|\lambda\,\boldsymbol{\alpha}\|^2}\right|} = \frac{\alpha_{\text{cut}}}{\sqrt{1-\lambda^2\,\alpha_{\text{cut}}^2}}. \tag{160}$$

Combining these 3 possibilities:

$$\max_{\boldsymbol{\alpha}\in\Xi} \frac{\|\boldsymbol{\alpha}\|_\infty}{\left|\sqrt{1-\|\lambda\,\boldsymbol{\alpha}\|^2}\right|} = \frac{\min(\alpha_{\text{cut}}, \alpha_{\text{samp}})}{\sqrt{1-\lambda^2\,\min(\alpha_{\text{cut}}, \sqrt{2}\,\alpha_{\text{samp}})^2}}. \tag{161}$$

In principle, to avoid aliasing, the sampling step must be chosen so that the Nyquist frequency is not less than the cutoff frequency, that is $\alpha_{\text{samp}} \geq \alpha_{\text{cut}}$, so that the above right-hand side is given by Eq. (160). In this case the sampling conditions are:

$$\begin{cases} \dfrac{2\,\lambda\,\alpha_{\text{cut}}\,|z|\,\delta\alpha}{\sqrt{1-\lambda^2\,\alpha_{\text{cut}}^2}} = \dfrac{2\,\lambda\,\alpha_{\text{cut}}\,|z|}{N\,\delta x\,\sqrt{1-\lambda^2\,\alpha_{\text{cut}}^2}} \leq 1 \\ \delta x \leq \dfrac{1}{2\,\alpha_{\text{cut}}} \end{cases} \tag{162}$$

which can be combined in a bracketing condition for the sampling step δx:

$$\frac{2\,\lambda\,|z|\,\alpha_{\text{cut}}}{N\,\sqrt{1-\lambda^2\,\alpha_{\text{cut}}^2}} \leq \delta x \leq \frac{1}{2\,\alpha_{\text{cut}}}. \tag{163}$$

2.4.2 Propagation by the paraxial transfer function

In the paraxial conditions, the propagation transfer function is given by Eq. (55) which corresponds to frequencies much smaller than $1/\lambda$:

$$\widetilde{h}_z(\boldsymbol{\alpha}) \underset{\|\boldsymbol{\alpha}\|\ll 1/\lambda}{\approx} \mathrm{e}^{\mathrm{i}\,k\,z}\,\mathrm{e}^{-\mathrm{i}\,\pi\,\lambda\,z\,\|\boldsymbol{\alpha}\|^2}. \tag{164}$$

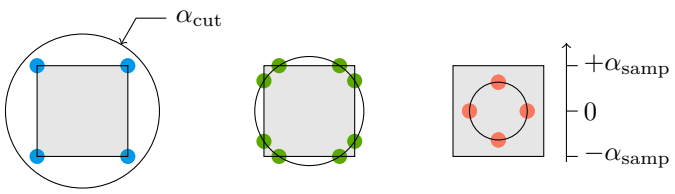

Figure 6: Spatial frequencies (indicated by colored circles) where the phase wrapping is the most severe for the non-paraxial propagation transfer function. For the 3 possible cases, the grayed square indicates the area sampled by the DFT with α_{samp} the Nyquist frequency, and the circle indicates the cutoff frequency α_{cut} of the angular spectrum assumed to be less the evanescent waves limit at $1/\lambda$.

The worst frequencies for the quadratic phase term $\phi(\boldsymbol{\alpha}) = \pi\,\lambda\,z\,\|\boldsymbol{\alpha}\|^2$ are such

$$\begin{aligned}
\delta\phi_{\max} &= \max_{\substack{\boldsymbol{\alpha}\in\Xi \\ \delta\boldsymbol{\alpha}\in\delta\Xi}} |\phi(\boldsymbol{\alpha}+\delta\boldsymbol{\alpha}) - \phi(\boldsymbol{\alpha})| && (165)\\
&= \pi\,\lambda\,|z| \max_{\substack{\boldsymbol{\alpha}\in\Xi \\ \delta\boldsymbol{\alpha}\in\delta\Xi}} \left| \|\boldsymbol{\alpha}+\delta\boldsymbol{\alpha}\|^2 - \|\boldsymbol{\alpha}\|^2 \right| && (166)\\
&= \pi\,\lambda\,|z| \max_{\substack{\boldsymbol{\alpha}\in\Xi \\ \delta\boldsymbol{\alpha}\in\delta\Xi}} \left| \|\delta\boldsymbol{\alpha}\|^2 + 2\,\langle\boldsymbol{\alpha},\delta\boldsymbol{\alpha}\rangle \right| && (167)\\
&= \pi\,\lambda\,|z| \left(\delta\alpha^2 + 2\,\delta\alpha \max_{\boldsymbol{\alpha}\in\Xi} \|\boldsymbol{\alpha}\|_\infty \right) && (168)\\
&\approx 2\,\pi\,\lambda\,|z|\,\delta\alpha \max_{\boldsymbol{\alpha}\in\Xi} \|\boldsymbol{\alpha}\|_\infty && (169)\\
&= 2\,\pi\,\lambda\,|z|\,\delta\alpha\,\min(\alpha_{\text{samp}}, \alpha_{\text{cut}}, 1/\lambda) && (170)
\end{aligned}$$

which (as expected) correspond to the conditions in Eq. (162) at low-frequencies.

$$\begin{cases}
\alpha_{\text{cut}} \ll 1/\lambda \\
\alpha_{\text{cut}} \leq \alpha_{\text{samp}} \\
2\,\lambda\,\alpha_{\text{cut}}\,|z|\,\delta\alpha = \dfrac{2\,\lambda\,\alpha_{\text{cut}}\,|z|}{N\,\delta x} \leq 1
\end{cases} \tag{171}$$

2.5 Propagation by the Fresnel transform

2.6 Discrete computations

See Sziklas and Siegman (1974) and Sziklas and Siegman (1975).

Several methods have been proposed for the numerical propagation of 2-dimensional sampled planar fields of size $N \times N$. Discrete approximation by a Riemann sum of the diffraction integral equation requires $\mathcal{O}(N^4)$ numerical floating-point operations, finite difference methods to numerically solve the differential Helmholtz equation is as demanding because of the number of steps to propagate the wave (Sziklas and Siegman, 1975). Using the Fast Fourier Transform (FFT) to compute the convolution product (the so-called angular spectrum method) requires $\mathcal{O}(N^2\,\log_2 N)$ operations

but imposes that the sampling steps δx in the transverse planes be the same along the propagation.

Angular spectrum propagation. In this method, the propagation between a transverse plane at z_0 to a transverse plane at $z_1 = z_0 + \Delta z$ is implemented by a discrete convolution of the field u_{z_0} by the shift-invariant propagation kernel $h_{\Delta z}$. For speed, the discrete convolution is computed by means of Fast Fourier Transforms (FFTs).

The sampled angular spectrum is given by:

$$\begin{aligned}\widetilde{\boldsymbol{u}}_z[\ell_1, \ell_2] &= \widetilde{u}_z(\alpha_x[\ell_1], \alpha_y[\ell_2]) \\ &= \iint u_z(x, y)\, \mathrm{e}^{-\mathrm{i}\, 2\, \pi\, (\alpha_x[\ell_1]\, x, \alpha_y[\ell_2]\, y)} \mathrm{d}x\, \mathrm{d}y \\ &\approx \sum_{k_1, k_2} u_z(x[j_1], y[j_2])\, \mathrm{e}^{-\mathrm{i}\, 2\, \pi\, (\alpha_x[\ell_1]\, x[j_1], \alpha_y[\ell_2]\, y[j_2])}\, |\delta x\, \delta y| \\ &= |\delta x\, \delta y|\, \big(\mathbf{F} \cdot \boldsymbol{u}_z\big)[\ell_1, \ell_2] \end{aligned} \tag{172}$$

where $\mathbf{F}$ is the forward DFT operator (see Appendix C), $\boldsymbol{u}_z$ is the sampled field $u_z(x, y)$ with sampling step sizes δx and δy along the x and y dimensions, and the square brackets are used to index the sampled quantities (as in the first line of the above equation). According to the properties of the DFT, the discrete angular spectrum $\widetilde{\boldsymbol{u}}_z$ is sampled with steps $\delta\alpha_x = 1/(N_1\, \delta x)$ and $\delta\alpha_y = 1/(N_2\, \delta y)$. In the following, we assume that the sampling steps and the number of samples are the same along the two transverse Cartesian axes so that: $N_1 = N_2 = N$ and $\delta x = \delta y$ and thus:

$$\widetilde{\boldsymbol{u}}_z = |\delta x|^2\, \mathbf{F} \cdot \boldsymbol{u}_z, \tag{173}$$

is the discrete angular spectrum with frequency sampling steps $\delta\alpha_x = \delta\alpha_y = 1/(N\, \delta x)$. Conversely:

$$\boldsymbol{u}_z = |\delta\alpha|^2\, \mathbf{F}^\star \cdot \widetilde{\boldsymbol{u}}_z, \tag{174}$$

where $\mathbf{F}^\star$, the adjoint of $\mathbf{F}$, is the backward DFT operator. It is easy to check that Eq. (174) with $\delta\alpha = 1/(N\, \delta x)$ is indeed the inverse of Eq. (173):

$$|\delta\alpha|^2\, \mathbf{F}^\star \cdot \widetilde{\boldsymbol{u}}_z = \frac{1}{(N\, |\delta x|)^2}\, \mathbf{F}^\star \cdot \big(|\delta x|^2\, \mathbf{F} \cdot \boldsymbol{u}_z\big) = \frac{1}{N^2}\, \mathbf{F}^\star \cdot \mathbf{F} \cdot \boldsymbol{u}_z = \boldsymbol{u}_z$$

where the last simplification follows from Eq. (**??**). The field in the transverse plane at z_1 knowing the field in the transverse plane at z_0 is given by:

$$\boldsymbol{u}_{z_1} = \frac{1}{N^2}\, \mathbf{F}^\star \cdot \mathrm{diag}\big(\widetilde{\boldsymbol{h}}_{z_1 - z_0}\big) \cdot \mathbf{F} \cdot \boldsymbol{u}_{z_0} \tag{175}$$

where $\mathrm{diag}(\boldsymbol{a})$ denotes a diagonal linear operator whose diagonal entries are those of $\boldsymbol{a}$ and such that applying this operator to, say, $\boldsymbol{b}$ yields the element-wise multiplication of $\boldsymbol{a}$ and $\boldsymbol{b}$. In the above equation, $\widetilde{\boldsymbol{h}}_{z_1 - z_0}$ is either the discrete Fourier transform, as defined in Eq. (173), of the propagation kernel $h_{z_1 - z_0}(x, y)$ sampled with steps of size δx or $\widetilde{h}_{z_1 - z_0}(\boldsymbol{\alpha})$ sampled with steps of size $\delta\alpha = 1/(N\, \delta x)$. Due to the approximation

of the continuous Fourier transform by the discrete transform, the two are not exactly equivalent.

The operator implementing the propagation by means of the angular spectrum writes:

$$\mathbf{H}_z^{\text{conv}} = \frac{1}{N^2}\,\mathbf{F}^\star \cdot \operatorname{diag}\left(\widetilde{\boldsymbol{h}}_z\right) \cdot \mathbf{F}. \tag{176}$$

With this method, the sampling steps are unchanged and the exact or paraxial planar propagation may be modeled. The methods considered next specifically implement Fresnel diffraction that is assuming the paraxial approximation.

To avoid aliasing, $\mathcal{D}_{1/\lambda}$ must be inside the support sampled by the discrete frequencies. Hence, the Nyquist frequency must not be smaller than $1/\lambda$ which writes:

$$(N/2)\,\delta\alpha \geq 1/\lambda \quad \Longleftrightarrow \quad \delta x \leq \lambda/2. \tag{177}$$

Single-FFT Fresnel propagation. In the paraxial approximation (Fresnel diffraction), the propagation kernel is given by Eq. (58) and the resulting field in transverse plane at $z_1 = z_0 + \Delta z$ is:

$$\begin{aligned} u_{z_1}(\boldsymbol{x}_1) &= \iint u_{z_0}(\boldsymbol{x}_0)\, h_{\Delta z}(\boldsymbol{x}_1 - \boldsymbol{x}_0)\,\mathrm{d}\boldsymbol{x}_0 \\ &= \frac{\mathrm{e}^{\mathrm{i}\,k\,\Delta z}}{\mathrm{i}\,\lambda\,\Delta z} \iint u_{z_0}(\boldsymbol{x}_0)\,\mathrm{e}^{\mathrm{i}\,k\,\frac{\|\boldsymbol{x}_1-\boldsymbol{x}_0\|^2}{2\,\Delta z}}\,\mathrm{d}\boldsymbol{x}_0 \\ &= \frac{\mathrm{e}^{\mathrm{i}\,k\,\Delta z}}{\mathrm{i}\,\lambda\,\Delta z}\,\mathrm{e}^{\mathrm{i}\,k\,\frac{\|\boldsymbol{x}_1\|^2}{2\,\Delta z}} \iint \left[u_{z_0}(\boldsymbol{x}_0)\,\mathrm{e}^{\mathrm{i}\,k\,\frac{\|\boldsymbol{x}_0\|^2}{2\,\Delta z}}\right] \mathrm{e}^{-\mathrm{i}\,k\,\frac{\langle \boldsymbol{x}_1,\boldsymbol{x}_0\rangle}{\Delta z}}\,\mathrm{d}\boldsymbol{x}_0 \end{aligned} \tag{178}$$

where the integral in the last right-hand side is similar to taking the Fourier transform of the term in square brackets. This integral can thus be computed by a single DFT provided the sampling condition in Eq. (235) holds which imposes that:

$$\frac{k\,\delta x_0\,\delta x_1}{\Delta z} = \pm\frac{2\,\pi}{N} \tag{179}$$

with N the number of samples along a transverse dimension. The sampling step in the output plane is thus given by:

$$\delta x_1 = \frac{\lambda\,|\Delta z|}{N\,\delta x_0} \tag{180}$$

and the double integral is approximated by $\delta x_0^2\,\mathbf{F}$ if $\Delta z > 0$ and by $\delta x_0^2\,\mathbf{F}^\star$ if $\Delta z < 0$ with $\mathbf{F}$ the 2-dimensional discrete Fourier transform operator (see Appendix C). Note that, with this latter convention, the transverse axes (x and y) keep their orientation.

Using bold lowercase symbols to represent sampled quantities and bold uppercase

symbols to represent operators, **single-FFT Fresnel propagation** writes:

$$\begin{aligned}
&\boldsymbol{u}_{z_1} = \frac{\delta x_0^2\, \mathrm{e}^{\mathrm{i}\, k\, \Delta z}}{\mathrm{i}\, \lambda\, \Delta z}\, \mathbf{Q}_{\frac{\delta x_1^2}{\lambda\, \Delta z}} \cdot \mathbf{F}_{\Delta z} \cdot \mathbf{Q}_{\frac{\delta x_0^2}{\lambda\, \Delta z}} \cdot \boldsymbol{u}_{z_0} \\
&\delta x_1 = \frac{\lambda\, |\Delta z|}{N\, \delta x_0} \\
&\Delta z = z_1 - z_0 \\
&\\
&\mathbf{F}_{\Delta z} = \begin{cases} \mathbf{F} & \text{if } \Delta z > 0, \\ \mathbf{F}^\star & \text{if } \Delta z < 0 \end{cases} \\
&\mathbf{Q}_\rho = \mathrm{diag}(\boldsymbol{q}_\rho) \quad \text{with} \quad \boldsymbol{q}_\rho[\boldsymbol{j}] = \mathrm{e}^{\mathrm{i}\, \pi\, \rho\, \|\boldsymbol{j}\|^2} \quad \forall \boldsymbol{j} \in \mathbb{J} \times \mathbb{J}
\end{aligned} \tag{181}$$

where operator $\mathbf{F}_{\Delta z}$ is to simplify the notation while operator $\mathbf{Q}_\rho$ implements element-wise multiplication by a quadratic phase factor. Note that multiplication by the scalar δx_0^2 commutes with all operators but that operators $\mathbf{F}_{\Delta z}$ and $\mathbf{Q}_\rho$ do not commute. Also note that $\boldsymbol{u}_{z_0}$ and $\boldsymbol{u}_{z_1}$ denote the complex amplitude in the transverse planes respectively at z_0 and z_1 and respectively sampled with steps δx_0 and δx_1 which are related by Eq. (180) and are usually not equal.

In continuous coordinates, the quadratic phase factors is given by:

$$\mathcal{Q}_\rho(\boldsymbol{x}) = \mathrm{e}^{\mathrm{i}\, \pi\, \rho\, \|\boldsymbol{x}\|^2}, \tag{182}$$

whose 2-dimensional Fourier transform is:

$$\widetilde{\mathcal{Q}}_\rho = \frac{\mathrm{i}}{\rho}\, \mathcal{Q}_{-1/\rho}. \tag{183}$$

Two-step Fresnel propagation. To circumvent the limitations of the Fresnel method, the propagation by Δz can be split in 2 steps, by $\Delta z'$ and then by $\Delta z''$ such that $\Delta z' + \Delta z'' = \Delta z$. By Eq. (180), the sampling steps, δx_m and δx_1, after these two Fresnel propagation steps are given by:

$$\delta x_\mathrm{m} = \frac{\lambda\, |\Delta z'|}{N\, \delta x_0}, \tag{184a}$$

$$\delta x_1 = \frac{\lambda\, |\Delta z''|}{N\, \delta x_\mathrm{m}} = \left| \frac{\Delta z''}{\Delta z'} \right| \delta x_0 = |\overline{\gamma}|\, \delta x_0 \tag{184b}$$

with (the minus sign is to simplify equations to come):

$$\overline{\gamma} = \frac{-\Delta z''}{\Delta z'}. \tag{185}$$

Hence an arbitrary magnification $\gamma = |\overline{\gamma}| = \delta x_1 / \delta x_0$ can be achieved by a 2-step Fresnel propagation with $\Delta z'$ and $\Delta z''$ given by:

$$\Delta z / \Delta z' = 1 - \overline{\gamma}, \tag{186a}$$

$$\Delta z / \Delta z'' = 1 - 1/\overline{\gamma}. \tag{186b}$$

Since $\overline{\gamma} = \pm\gamma$, there are 2 possible choices for a given magnification γ.

Using the operators notation, the 2-step Fresnel propagation yields the following sampled complex amplitude in the transverse plane at z_1:

$$\begin{aligned}
\boldsymbol{u}_{z_1} &= \frac{\mathrm{e}^{\mathrm{i}\,k\,\Delta z''}}{\mathrm{i}\,\lambda\,\Delta z''}\,\mathbf{Q}_{\frac{\delta x_1^2}{\lambda\,\Delta z''}}\cdot\delta x_\mathrm{m}^2\,\mathbf{F}_{\Delta z''}\cdot\mathbf{Q}_{\frac{\delta x_\mathrm{m}^2}{\lambda\,\Delta z''}}\cdot\boldsymbol{u}_{z_\mathrm{m}} \\
&= \frac{\mathrm{e}^{\mathrm{i}\,k\,\left(\Delta z'+\Delta z''\right)}}{\left(\mathrm{i}\,\lambda\right)^2\,\Delta z'\,\Delta z''}\,\delta x_\mathrm{m}^2\,\delta x_0^2\,\mathbf{Q}_{\frac{\delta x_1^2}{\lambda\,\Delta z''}}\cdot\mathbf{F}_{\Delta z''}\cdot\mathbf{Q}_{\frac{\delta x_\mathrm{m}^2}{\lambda}\left(\frac{1}{\Delta z''}+\frac{1}{\Delta z'}\right)}\cdot\mathbf{F}_{\Delta z'}\cdot\mathbf{Q}_{\frac{\delta x_0^2}{\lambda\,\Delta z'}}\cdot\boldsymbol{u}_{z_0} \\
&= \frac{-\mathrm{e}^{\mathrm{i}\,k\,\Delta z}}{N^2}\,\frac{\Delta z'}{\Delta z''}\,\mathbf{Q}_{\frac{\delta x_1^2}{\lambda\,\Delta z''}}\cdot\mathbf{F}_{\Delta z''}\cdot\mathbf{Q}_{\frac{\delta x_\mathrm{m}^2}{\lambda}\left(\frac{1}{\Delta z''}+\frac{1}{\Delta z'}\right)}\cdot\mathbf{F}_{\Delta z'}\cdot\mathbf{Q}_{\frac{\delta x_0^2}{\lambda\,\Delta z'}}\cdot\boldsymbol{u}_{z_0}
\end{aligned} \tag{187}$$

where $z_\mathrm{m} = z_0 + \Delta z'$ is the position of the intermediate transverse plane. Then using, Eqs. (184a), (184b), (186a) and (186b), the sampled complex amplitude obtained by the 2-step Fresnel propagation writes:

$$\boldsymbol{u}_{z_1} = \frac{\mathrm{e}^{\mathrm{i}\,k\,\Delta z}}{\overline{\gamma}\,N^2}\,\mathbf{Q}_{\frac{\overline{\gamma}\,(\overline{\gamma}-1)\,\delta x_0^2}{\lambda\,\Delta z}}\cdot\mathbf{F}_{\Delta z''}\cdot\mathbf{Q}_{\frac{-\lambda\,\Delta z}{\overline{\gamma}\,N^2\,\delta x_0^2}}\cdot\mathbf{F}_{\Delta z'}\cdot\mathbf{Q}_{\frac{(1-\overline{\gamma})\,\delta x_0^2}{\lambda\,\Delta z}}\cdot\boldsymbol{u}_{z_0} \tag{188}$$

with the same operators as defined in Eq. (181).

Note that, if the same step size is chosen, then $\gamma = 1$ and $\overline{\gamma} = \pm 1$. However, taking $\overline{\gamma} = 1$ and since $\mathbf{Q}_0 = \mathbf{I}$ the identity, the propagated complex visibility writes:

$$\boldsymbol{u}_{z_1} = \frac{\mathrm{e}^{\mathrm{i}\,k\,\Delta z}}{N^2}\,\mathbf{F}_{\Delta z''}\cdot\mathbf{Q}_{\frac{-\lambda\,\Delta z}{N^2\,\delta x_0^2}}\cdot\mathbf{F}_{\Delta z'}\cdot\boldsymbol{u}_{z_0} \tag{189}$$

which is the expression computed using the angular spectrum (check this, notably FFT direction).

To relax a bit anti-aliasing conditions, one should account for the limited spectral bandwidth of the angular spectrum and for the limited beam size.

To avoid aliasing in the central quadratic phase factor of Eq. (188) the following condition must hold:

$$\left|\frac{\lambda\,\Delta z}{\overline{\gamma}\,N^2\,\delta x_0^2}\right| \leq \frac{1}{N} \quad\Longleftrightarrow\quad \gamma = |\overline{\gamma}| \geq \frac{\lambda\,|\Delta z|}{N\,\delta x_0^2} \tag{190}$$

Furthermore, assuming the wavefront of $\boldsymbol{u}_{z_0}$ has a curvature $1/R_0$, avoiding aliasing in the rightmost quadratic phase factor imposes that:

$$\left|\frac{\delta x_0^2}{\lambda}\left(\frac{1-\overline{\gamma}}{\Delta z}+\frac{1}{R_0}\right)\right| \leq \frac{1}{N} \quad\Longleftrightarrow\quad 1+\frac{\Delta z}{R_0}-\frac{\lambda\,|\Delta z|}{N\,\delta x_0^2} \leq \overline{\gamma} \leq 1+\frac{\Delta z}{R_0}+\frac{\lambda\,|\Delta z|}{N\,\delta x_0^2} \tag{191}$$

For a plane input wavefront, *i.e.* $1/R_0 = 0$, with $\lambda = 500\,\mathrm{nm}$, $\delta x_0 = 0.1\,\mathrm{mm}$, $|\Delta z| = 10\,\mathrm{cm}$, and $N = 1024$, conditions in Eqs. (190) and (191) are $|\overline{\gamma}| \geq 48.8$ and $-47.8 \leq \overline{\gamma} \leq 49.8$. Combining the two yields $48.8 \leq \overline{\gamma} \leq 49.8$ which is quite restrictive and leads to have $\delta x_1 \in [4.88, 4.98]\,\mathrm{mm}$.

Angular spectrum propagation with magnification. In his book, Schmidt (2010) recalls the approach of Tyler and Fried (1982) and Roberts (1986) who rewrote the Fresnel propagation integral so as to be able to change the sampling rate of the result. Their idea is that, to have a sampling step δx_1 in the output transverse plane at z_1 that is different from the sampling step δx_0 in the input transverse plane at z_0, Fresnel propagation integral in Eq. (59) should be rewritten to yield $u'_{z_1}(\boldsymbol{x}'_1) = u_{z_1}(\gamma\,\boldsymbol{x}'_1)$ with $\boldsymbol{x}'_1 = \boldsymbol{x}_1/\gamma$ and $\gamma = \delta x_1/\delta x_0$ the desired magnification. Their method is detailed next.

Using the identity:

$$\|\boldsymbol{x}_1 - \boldsymbol{x}_0\|^2 = \gamma\,\|\boldsymbol{x}_1/\gamma - \boldsymbol{x}_0\|^2 + (1-\gamma)\,\|\boldsymbol{x}_0\|^2 + (1-1/\gamma)\,\|\boldsymbol{x}_1\|^2 \tag{192}$$

which holds for any $\gamma \neq 0$ as is easily proven by expanding the squares, the Fresnel propagation equation in Eq. (59) can be rewritten as:

$$\begin{aligned} u_{z_1}(\boldsymbol{x}_1) &= \frac{\mathrm{e}^{\mathrm{i}\,k\,\Delta z}}{\mathrm{i}\,\lambda\,\Delta z} \iint u_{z_0}(\boldsymbol{x}_0)\,\mathrm{e}^{\frac{\mathrm{i}\,k\,\|\boldsymbol{x}_1-\boldsymbol{x}_0\|^2}{2\,\Delta z}}\,\mathrm{d}\boldsymbol{x}_0 \\ &= \frac{\mathrm{e}^{\mathrm{i}\,k\,\Delta z}}{\mathrm{i}\,\lambda\,\Delta z}\,\mathrm{e}^{\frac{\mathrm{i}\,k\,(1-1/\gamma)\,\|\boldsymbol{x}_1\|^2}{2\,\Delta z}} \iint \left[u_{z_0}(\boldsymbol{x}_0)\,\mathrm{e}^{\frac{\mathrm{i}\,k\,(1-\gamma)\,\|\boldsymbol{x}_0\|^2}{2\,\Delta z}}\right] \mathrm{e}^{\frac{\mathrm{i}\,k\,\gamma\,\|\boldsymbol{x}_1/\gamma-\boldsymbol{x}_0\|^2}{2\,\Delta z}}\,\mathrm{d}\boldsymbol{x}_0 \end{aligned} \tag{193}$$

Then, with $\boldsymbol{x}'_1 = \boldsymbol{x}_1/\gamma$, $u'_{z_1}(\boldsymbol{x}'_1) = u_{z_1}(\gamma\,\boldsymbol{x}'_1)$ and:

$$u''_{z_0}(\boldsymbol{x}_0) = u_{z_0}(\boldsymbol{x}_0)\,\mathrm{e}^{\frac{\mathrm{i}\,k\,(1-\gamma)\,\|\boldsymbol{x}_0\|^2}{2\,\Delta z}} = u_{z_0}(\boldsymbol{x}_0)\,\mathrm{e}^{\mathrm{i}\,\pi\,\frac{(1-\gamma)\,\|\boldsymbol{x}_0\|^2}{\lambda\,\Delta z}},$$

the Fresnel propagation equation becomes:

$$u'_{z_1}(\boldsymbol{x}'_1) = \frac{\mathrm{e}^{\mathrm{i}\,k\,\Delta z}}{\mathrm{i}\,\lambda\,\Delta z}\,\mathrm{e}^{\frac{\mathrm{i}\,\pi\,\gamma\,(\gamma-1)\,\|\boldsymbol{x}'_1\|^2}{\lambda\,\Delta z}} \iint u''_{z_0}(\boldsymbol{x}_0)\,\mathrm{e}^{\frac{\mathrm{i}\,k\,\gamma\,\|\boldsymbol{x}'_1-\boldsymbol{x}_0\|^2}{2\,\Delta z}}\,\mathrm{d}\boldsymbol{x}_0 \tag{194}$$

where the integral reads as the convolution of $u''_{z_0}(\boldsymbol{x}_0)$ by the kernel:

$$h(\boldsymbol{x}) = \mathrm{e}^{\frac{\mathrm{i}\,k\,\gamma\,\|\boldsymbol{x}\|^2}{2\,\Delta z}}. \tag{195}$$

Using Eqs. (55) and (58), the Fourier transform of this kernel is:

$$\widetilde{h}(\boldsymbol{\alpha}) = \frac{\mathrm{i}\,\lambda\,\Delta z}{\gamma}\,\mathrm{e}^{-\mathrm{i}\,\pi\,\lambda\,\|\boldsymbol{\alpha}\|^2\,\Delta z/\gamma}, \tag{196}$$

which may be used to rewrite the convolution as the inverse Fourier transform of the product of $\widetilde{u}''_{z_0}(\boldsymbol{\alpha})$, the Fourier transform of $u''_{z_0}(\boldsymbol{x}_0)$, and of $\widetilde{h}(\boldsymbol{\alpha})$:

$$u'_{z_1}(\boldsymbol{x}'_1) = \frac{\mathrm{e}^{\mathrm{i}\,k\,\Delta z}}{\gamma}\,\mathrm{e}^{\frac{\mathrm{i}\,\pi\,\gamma\,(\gamma-1)\,\|\boldsymbol{x}'_1\|^2}{\lambda\,\Delta z}}\,\mathcal{F}^{-1}\left\{\widetilde{u}''_{z_0}(\boldsymbol{\alpha})\,\mathrm{e}^{-\mathrm{i}\,\pi\,\lambda\,\|\boldsymbol{\alpha}\|^2\,\Delta z/\gamma}\,\middle|\,\boldsymbol{\alpha} \to \boldsymbol{x}'_1\right\}. \tag{197}$$

Using discrete Fourier transforms (DFTs) and sampled complex amplitudes to approximate the above equation yields $\boldsymbol{u}'_{z_1}$, the complex amplitude $u'_{z_1}(\boldsymbol{x}'_1)$ sampled with a step $\delta x'_1 = \delta x_0$ because the convolution has been approximated by DFTs. Since $u'_{z_1}(\boldsymbol{x}'_1) = u_{z_1}(\gamma\,\boldsymbol{x}'_1)$, $\boldsymbol{u}'_{z_1}$ is also $\boldsymbol{u}_{z_1}$, the complex amplitude $u_{z_1}(\boldsymbol{x}_1)$ sampled

with a step $\delta x_1 = \gamma\,\delta x_1' = \gamma\,\delta x_0$. Hence, by rewriting Fresnel propagation with the angular spectrum (because a convolution has been used) as described above, an arbitrary magnification $\gamma = \delta x_1/\delta x_0$ can be chosen. Using the discrete operators previously introduced the complex amplitude in transverse plane at z_1 sampled with step $\delta x_1 = \gamma\,\delta x_0$ writes:

$$\boxed{\boldsymbol{u}_{z_1} = \frac{\mathrm{e}^{\mathrm{i}\,k\,\Delta z}}{\gamma\,N^2}\,\mathbf{Q}_{\frac{\gamma\,(\gamma-1)\,\delta x_0^2}{\lambda\,\Delta z}}\cdot\mathbf{F}^{\star}\cdot\mathbf{Q}_{\frac{-\lambda\,\Delta z}{\gamma\,N^2\,\delta x_0^2}}\cdot\mathbf{F}\cdot\mathbf{Q}_{\frac{(1-\gamma)\,\delta x_0^2}{\lambda\,\Delta z}}\cdot\boldsymbol{u}_{z_0}} \tag{198}$$

where it has been accounted for $\delta\alpha = 1/(N\,\delta x_0)$ according to Eq. (231) and with $\Delta z = z_1 - z_0$.

Note that, taking $\overline{\gamma} = \gamma$ in the 2-step Fresnel propagation in Eq. (188) exactly yields Eq. (198) provided $\Delta z' > 0$ and $\Delta z'' < 0$. The fact that $\Delta z'' = -\overline{\gamma}\,\Delta z'$ warrants that $\Delta z'$ and $\Delta z''$ have opposite signs when $\overline{\gamma} = \gamma > 0$. Check that this does not make any difference because the direct and inverse Fourier transform of the Fresnel propagation kernel are the same, due to its Gaussian structure.

Fractional Fourier transform. Mas et al. (1999) proposed to use the fractional Fourier transform (FRFT) to perform Fresnel propagation by the same numerical method in the near and far fields. The resulting general expression, Eq. (18) in their paper, is an instance of the two-step paraxial propagation method.

In Mas et al. (1999), the propagation kernel is approximated by:

$$h_z^{\mathrm{Mas}}(x,y) = \exp\!\left(\mathrm{i}\,\pi\,\frac{x^2+y^2}{\lambda\,z}\right). \tag{199}$$

which, compared to Eq. (58), omits the factor $\exp(\mathrm{i}\,k\,z)/(\mathrm{i}\,\lambda\,z)$. This factor is needed to take into account the dilution of the amplitude and the optical path delay with the propagation distance z. Accounting for this phase delay may be important for modeling optical setups, such as interferometers, where the wave propagates along different interfering arms.

3 Optical components

Except when explicitly stated, diffraction by planar surfaces under the paraxial conditions (*i.e.* Fresnel diffraction) will be always be assumed.

3.1 Point source

From Eq. (26), a point source at position $\boldsymbol{r}_0 = (x_0, y_0, z_0)$ simply yields a field proportional to $h_{z-z_0}(x - x_0, y - y_0)$ at position $\boldsymbol{r} = (x, y, z)$ with $h_{\Delta z}$ the propagation kernel.

3.2 Thin lens

To model the effects of a thin lens of focal length f (positive for a converging lens, negative for a diverging lens) whose center is at $\boldsymbol{r}_\mathrm{c} = (x_\mathrm{c}, y_\mathrm{c}, z_\mathrm{c})$, we consider its effect on a point source at the front focal point of the lens, hence at position $\boldsymbol{r}_\mathrm{c} - f\,\boldsymbol{e}_z = (x_\mathrm{c}, y_\mathrm{c}, z_\mathrm{c} - f)$. In the transverse plane at z_c and just before the lens, the field is the one produced by the point source (see Section 3.1):

$$u_\mathrm{in}(\boldsymbol{x}) \propto h_f(\boldsymbol{x} - \boldsymbol{x}_\mathrm{c}) \propto \mathrm{e}^{\mathrm{i}\,k\,\frac{\|\boldsymbol{x}-\boldsymbol{x}_\mathrm{c}\|^2}{2\,f}}$$

where paraxial conditions have been assumed. Just after the lens, the wave should be planar, hence the effects of the thin lens is to add or subtract a quadratic phase to the incoming wavefront. The output field (after the lens) is thus given by:

$$u_\mathrm{out}(x, y) = u_\mathrm{in}(x, y)\,\mathrm{e}^{\mathrm{i}\,k\left[\ell - \frac{\|\boldsymbol{x}-\boldsymbol{x}_\mathrm{c}\|^2}{2\,f}\right]} \tag{200}$$

for any input field u_out (before the lens) and with $\ell \geq 0$ an optical path length accounting for the thickness of the lens:

$$\ell = \frac{n_\mathrm{glass}}{n}\,\ell_\mathrm{c} \tag{201}$$

with n and n_glass the respective refractive indices of the propagation medium and of the lens material and where ℓ_c is the physical thickness of the lens at its center.

What if the lens is tilted? Answer: move the point source at the actual position of the focus.

A The field as a superposition of plane waves

It is possible to find a family of solutions of the Helmholtz equation that are separable in Cartesian coordinates $\boldsymbol{r} = (x, y, z)$. Taking $u(x, y, z) = f_x(x)\, f_y(y)\, f_z(z)$ in Eq. (6) and dividing by $u(x, y, z)$, assuming it is not zero, yields:

$$\frac{f_x''(x)}{f_x(x)} + \frac{f_y''(y)}{f_y(y)} + \frac{f_z''(z)}{f_z(z)} + k^2 = 0.$$

In the right-hand side expression, the first term only depends on x, the second term only depends on y, the third term only depends on z, and the fourth term is constant. Hence all these terms must be constant, so that Helmholtz equation amounts to:

$$\begin{cases} f_x''(x) = \rho_x\, f_x(x) \\ f_y''(y) = \rho_y\, f_y(y) \\ f_z''(z) = \rho_z\, f_z(z) \end{cases} \qquad \text{subject to} \quad \rho_x + \rho_y + \rho_z + k^2 = 0$$

with $(\rho_x, \rho_y, \rho_z) \in \mathbb{R}^3$. For a given component, say f_x, the possible solutions depend on the sign of ρ_x:

- If $\rho_x > 0$, introducing $\mu_x = \sqrt{\rho_x} > 0$, the solution is a linear combination of $\exp(\mu_x\, x)$ and of $\exp(-\mu_x\, x)$. These particular solutions are amplified exponentially while they propagate in a direction such that x is respectively increasing or decreasing. This is impossible in the absence of sources. Hence, the only physically possible solution is a linear combination of the exponentially damped particular solutions:

  $$f_x(x) = f_x(x_0)\, \mathrm{e}^{-\mu_x\, |x - x_0|}$$

  which is rapidly vanishing with the distance $|x - x_0|$ and is called an **evanescent wave**.

- If $\rho_x \leq 0$, the solution is a linear combination of $\exp(\mathrm{i}\, k_x\, x)$ with $k_x = \pm\sqrt{-\rho_x}$ so that $k_x^2 = -\rho_x$. In that case, $f_x(x)$ is a sinusoidal function of x with wave number $|k_x|$.

The general solution to the Helmholtz equation (6), that is the field $u(x, y, z)$, is a superposition of all possible particular solutions which, neglecting the evanescent waves, are given by:

$$\mathrm{e}^{\mathrm{i}\,(k_x\, x + k_y\, y + k_z\, z)} \quad \text{such that} \quad k_x^2 + k_y^2 + k_z^2 = k^2. \tag{202}$$

In other words and neglecting the evanescent waves, the field $u(\boldsymbol{r})$ can be written as the superposition of mono-chromatic plane waves propagating as $\exp(\mathrm{i}\, \boldsymbol{k} \cdot \boldsymbol{r})$ with wave vector $\boldsymbol{k} = (k_x, k_y, k_z)$ and such that $\left\|\boldsymbol{k}\right\| = k = 2\,\pi/\lambda$. Owing to this latter constraint that holds for a mono-chromatic wave, there are only 2 free parameters

out of k_x, k_y, and k_z. For instance, taking $k_z = \pm\sqrt{k^2 - k_x^2 - k_y^2}$, the most general expression for the superposition of the mono-chromatic plane waves is given by:

$$u(x,y,z) = \iint_{\mathcal{D}_k} \left[a(k_x,k_y)\, \mathrm{e}^{+\mathrm{i}\sqrt{k^2-k_x^2-k_y^2}\, z} + b(k_x,k_y)\, \mathrm{e}^{-\mathrm{i}\sqrt{k^2-k_x^2-k_y^2}\, z} \right] \times \mathrm{e}^{\mathrm{i}\,(k_x\, x + k_y\, y)}\, \mathrm{d}k_x\, \mathrm{d}k_y \tag{203}$$

where $a(k_x, k_y)$ and $b(k_x, k_y)$ are the weights of the superposition and:

$$\mathcal{D}_k = \left\{ (k_x, k_y) \in \mathbb{R}^2 \mid k_x^2 + k_y^2 \leq k^2 \right\} \tag{204}$$

is the disk of radius k centered at $(0, 0)$.

Note that, in Eq. (203), the choice of the axes of the Cartesian frame are arbitrary and that boundary conditions may apply to yield a more specific expression for the propagating field. See for example Section 1.5.2 "*Angular Spectrum*" where, using the angular spectrum, the very general solution in Eq. (203) can be restricted and simplified if we assume known the field in a plane defined by, say, $z = z_0$.

B Tilted paraxial approximation

Following the idea of a carrier wave, we consider that the propagating field $u_0(\boldsymbol{x})$ has a tilted wavefront compared to $a_0(\boldsymbol{x})$:

$$u_0(\boldsymbol{x}) = a_0(\boldsymbol{x})\,\mathrm{e}^{\mathrm{i}\,2\,\pi\,\boldsymbol{\beta}^\top\cdot\boldsymbol{x}} \tag{205}$$

with $\boldsymbol{\beta}$ the wavefront slope. The angular spectrum of $u_0(\boldsymbol{x})$ is then:

$$\widetilde{u}_0(\boldsymbol{\alpha}) = \iint a_0(\boldsymbol{x})\,\mathrm{e}^{-\mathrm{i}\,2\,\pi\,(\boldsymbol{\alpha}-\boldsymbol{\beta})^\top\cdot\boldsymbol{x}}\,\mathrm{d}\boldsymbol{x} = \widetilde{a}_0(\boldsymbol{\alpha}-\boldsymbol{\beta}), \tag{206}$$

that is the angular spectrum of $a_0(\boldsymbol{x})$ shifted by $\boldsymbol{\beta}$. The propagation of the field $u_0(\boldsymbol{x})$ then writes:

$$\begin{aligned}
u_z(\boldsymbol{x}) &= \iint \widetilde{u}_0(\boldsymbol{\alpha})\,\widetilde{h}_z(\boldsymbol{\alpha})\,\mathrm{e}^{\mathrm{i}\,2\,\pi\,\boldsymbol{\alpha}^\top\cdot\boldsymbol{x}}\,\mathrm{d}\boldsymbol{\alpha} \\
&= \iint \widetilde{a}_0(\boldsymbol{\alpha}-\boldsymbol{\beta})\,\widetilde{h}_z(\boldsymbol{\alpha})\,\mathrm{e}^{\mathrm{i}\,2\,\pi\,\boldsymbol{\alpha}^\top\cdot\boldsymbol{x}}\,\mathrm{d}\boldsymbol{\alpha} \\
&= \iint \widetilde{a}_0(\boldsymbol{\alpha})\,\widetilde{h}_z(\boldsymbol{\alpha}+\boldsymbol{\beta})\,\mathrm{e}^{\mathrm{i}\,2\,\pi\,(\boldsymbol{\alpha}+\boldsymbol{\beta})^\top\cdot\boldsymbol{x}}\,\mathrm{d}\boldsymbol{\alpha} \\
&= \mathrm{e}^{\mathrm{i}\,2\,\pi\,\boldsymbol{\beta}^\top\cdot\boldsymbol{x}} \iint \widetilde{a}_0(\boldsymbol{\alpha})\,\widetilde{h}_z(\boldsymbol{\alpha}+\boldsymbol{\beta})\,\mathrm{e}^{\mathrm{i}\,2\,\pi\,\boldsymbol{\alpha}^\top\cdot\boldsymbol{x}}\,\mathrm{d}\boldsymbol{\alpha} \\
&= a_z(\boldsymbol{x};\boldsymbol{\beta})\,\mathrm{e}^{\mathrm{i}\,2\,\pi\,\boldsymbol{\beta}^\top\cdot\boldsymbol{x}},
\end{aligned} \tag{207}$$

where:

$$a_z(\boldsymbol{x}) = \iint \widetilde{a}_0(\boldsymbol{\alpha})\,\widetilde{h}_z(\boldsymbol{\alpha}+\boldsymbol{\beta})\,\mathrm{e}^{\mathrm{i}\,2\,\pi\,\boldsymbol{\alpha}^\top\cdot\boldsymbol{x}}\,\mathrm{d}\boldsymbol{\alpha} \tag{208}$$

and with $\widetilde{h}_z(\boldsymbol{\alpha})$ the angular spectrum transfer function implementing the propagation between two transverse planes separated by an algebraic distance of z. With the convention that $z > 0$ in the direction of wave propagation, the transfer function is given by Eq. (44) and can be expressed as:

$$\widetilde{h}_z(\boldsymbol{\alpha}) = \mathrm{e}^{\mathrm{i}\,k\,z\,\rho(\boldsymbol{\alpha})} \tag{209}$$

with:

$$\rho(\boldsymbol{\alpha}) = \sqrt{1 - \|\lambda\,\boldsymbol{\alpha}\|^2}. \tag{210}$$

Angular spectrum propagation yields a solution to the Helmholtz equations with no approximations but it may be simpler to consider a low frequency approximation. Assuming $\widetilde{a}_0(\boldsymbol{\alpha})$ is negligible at high frequencies, Eq. (**??**) suggests to approximate the transfer function near the angular frequency $\boldsymbol{\beta}$ for a low frequency perturbation $\boldsymbol{\alpha}$. For that we need to approximate $\rho(\boldsymbol{\alpha}+\boldsymbol{\beta})$ for a given $\boldsymbol{\beta}$. The gradient and Hessian of $\rho(\boldsymbol{\alpha})$ are:

$$\nabla\rho(\boldsymbol{\alpha}) = \frac{-\lambda^2}{\rho(\boldsymbol{\alpha})}\,\boldsymbol{\alpha}, \tag{211}$$

$$\nabla^2\rho(\boldsymbol{\alpha}) = \frac{-\lambda^2}{\rho(\boldsymbol{\alpha})}\,\mathbf{I} - \frac{\lambda^4}{\rho(\boldsymbol{\alpha})^3}\,\boldsymbol{\alpha}\cdot\boldsymbol{\alpha}^\top, \tag{212}$$

where $\mathbf{I}$ is the 2×2 identity, $\boldsymbol{\alpha}^\top$ denotes the transpose of $\boldsymbol{\alpha}$, and, thus, $\boldsymbol{\alpha} \cdot \boldsymbol{\alpha}^\top$ is a rank-1 2×2 matrix. These derivatives lead to the following 2nd order series:

$$\begin{aligned}\rho(\boldsymbol{\alpha}+\boldsymbol{\beta}) &= \rho(\boldsymbol{\beta}) + \boldsymbol{\alpha}^\top \cdot \nabla\rho(\boldsymbol{\beta}) + \frac{1}{2}\,\boldsymbol{\alpha}^\top \cdot \nabla^2\rho(\boldsymbol{\beta}) \cdot \boldsymbol{\alpha} + \dots \\ &= \rho(\boldsymbol{\beta}) - \frac{\lambda^2\,\boldsymbol{\beta}^\top \cdot \boldsymbol{\alpha}}{\rho(\boldsymbol{\beta})} - \frac{\lambda^2\,\|\boldsymbol{\alpha}\|^2}{2\,\rho(\boldsymbol{\beta})} - \frac{\lambda^4\,\left(\boldsymbol{\beta}^\top \cdot \boldsymbol{\alpha}\right)^2}{2\,\rho(\boldsymbol{\beta})^3} + \dots \end{aligned} \tag{213}$$

If $\|\boldsymbol{\alpha}\|$ and $\|\boldsymbol{\beta}\|$ are both small compared to $1/\lambda$, then $\|\lambda\,\boldsymbol{\alpha}\| \ll 1$, $\|\lambda\,\boldsymbol{\beta}\| \ll 1$, and $\rho(\boldsymbol{\beta}) \approx 1$. In these conditions, the terms of the right-hand side of Eq. (213) can be ordered in magnitude as explained next. A first consequence of assuming that $\|\lambda\,\boldsymbol{\alpha}\| \ll 1$ and $\|\lambda\,\boldsymbol{\beta}\| \ll 1$ is:

$$\left|\lambda^2\,\boldsymbol{\beta}^\top \cdot \boldsymbol{\alpha}\right| \leq \|\lambda\,\boldsymbol{\alpha}\|\,\|\lambda\,\boldsymbol{\beta}\| \ll 1 \quad\Longrightarrow\quad \left|\lambda^2\,\boldsymbol{\beta}^\top \cdot \boldsymbol{\alpha}\right|^2 \ll \left|\lambda^2\,\boldsymbol{\beta}^\top \cdot \boldsymbol{\alpha}\right|, \tag{214}$$

hence, and since $\rho(\boldsymbol{\beta}) \approx 1$, the fourth term in the right-hand side of Eq. (213) is negligible compared to the second one. Another consequence of assuming that $\|\lambda\,\boldsymbol{\beta}\| \ll 1$ is:

$$\lambda^4\left|\boldsymbol{\beta}^\top \cdot \boldsymbol{\alpha}\right|^2 \leq \|\lambda\,\boldsymbol{\alpha}\|^2\,\|\lambda\,\boldsymbol{\beta}\|^2 \ll \|\lambda\,\boldsymbol{\alpha}\|^2, \tag{215}$$

which shows that the fourth term in the right-hand side of Eq. (213) is negligible compared to the third one. For instance, taking $\|\lambda\,\boldsymbol{\alpha}\| = \|\lambda\,\boldsymbol{\beta}\| = 0.3$ yields:

$$\begin{aligned} \rho(\boldsymbol{\beta}) &\simeq 0.95, \\ \frac{\lambda^2\left|\boldsymbol{\beta}^\top \cdot \boldsymbol{\alpha}\right|}{\rho(\boldsymbol{\beta})} \leq \frac{\|\lambda\,\boldsymbol{\alpha}\|\,\|\lambda\,\boldsymbol{\beta}\|}{\rho(\boldsymbol{\beta})} &\simeq 0.094, \\ \frac{\lambda^2\,\|\boldsymbol{\alpha}\|^2}{2\,\rho(\boldsymbol{\beta})} &\simeq 0.047, \\ \frac{\lambda^4\,\left(\boldsymbol{\beta}^\top \cdot \boldsymbol{\alpha}\right)^2}{2\,\rho(\boldsymbol{\beta})^3} \leq \frac{\|\lambda\,\boldsymbol{\alpha}\|^2\,\|\lambda\,\boldsymbol{\beta}\|^2}{2\,\rho(\boldsymbol{\beta})^3} &\simeq 0.0047. \end{aligned}$$

To summarize, if $\|\boldsymbol{\alpha}\|$ and $\|\boldsymbol{\beta}\|$ are both small compared to $1/\lambda$, the fourth term in the right-hand side of Eq. (213) can be neglected which leads to the following approximation:

$$\rho(\boldsymbol{\alpha}+\boldsymbol{\beta}) \approx \rho(\boldsymbol{\beta}) - \frac{\lambda^2\,\boldsymbol{\beta}^\top \cdot \boldsymbol{\alpha}}{\rho(\boldsymbol{\beta})} - \frac{\|\lambda\,\boldsymbol{\alpha}\|^2}{2\,\rho(\boldsymbol{\beta})}. \tag{216}$$

Compared to the paraxial approximation, there is a division by $\rho(\boldsymbol{\beta}) \approx 1$ and a linear term in $\boldsymbol{\alpha}$.

Using the approximation in Eq. (216), the transfer function becomes:

$$\widetilde{h}_z(\boldsymbol{\alpha}+\boldsymbol{\beta}) \approx \mathrm{e}^{\,\mathrm{i}\,k\,z\left(\rho(\boldsymbol{\beta}) - \frac{\lambda^2\,\boldsymbol{\beta}^\top \cdot \boldsymbol{\alpha}}{\rho(\boldsymbol{\beta})} - \frac{\|\lambda\,\boldsymbol{\alpha}\|^2}{2\,\rho(\boldsymbol{\beta})}\right)}, \tag{217}$$

Note that for $\boldsymbol{\beta} = \mathbf{0}$, then $\rho(\boldsymbol{\beta}) = 1$ and the usual paraxial approximation is retrieved, see Eq. (55). Considering the above expression, the fourth term in the right-hand side of Eq. (213) cannot be neglected if it induces a significant change of phase. This imposes that:

$$\left|k\,z\,\frac{\lambda^4\,\left(\boldsymbol{\beta}^\top \cdot \boldsymbol{\alpha}\right)^2}{2\,\rho(\boldsymbol{\beta})^3}\right| \ll \pi \quad\Longrightarrow\quad \|\lambda\,\boldsymbol{\alpha}\|\,\|\lambda\,\boldsymbol{\beta}\| \ll \sqrt{\frac{\lambda\,\rho(\boldsymbol{\beta})^3}{z}} \tag{218}$$

which may be much more restrictive than the conditions, $\|\lambda\,\boldsymbol{\alpha}\| \ll 1$ and $\|\lambda\,\boldsymbol{\beta}\| \ll 1$, for the pproximation in Eq. (216) to hold.

The right-hand side of Eq. (208) can be put in the form of a convolution of $a_0(\boldsymbol{x})$ by a kernel, say $h_z(\boldsymbol{x};\boldsymbol{\beta})$, resulting from the 2-dimensional Fourier transform in $\boldsymbol{\alpha}$ of $\widetilde{h}_z(\boldsymbol{\alpha}+\boldsymbol{\beta})$. Using the approximation in Eq. (216) this kernel writes:

$$\begin{aligned} h_z(\boldsymbol{x};\boldsymbol{\beta}) &= \iint \widetilde{h}_z(\boldsymbol{\alpha}+\boldsymbol{\beta})\,\mathrm{e}^{\mathrm{i}\,2\,\pi\,\boldsymbol{\alpha}^\top\cdot\boldsymbol{x}}\,\mathrm{d}\boldsymbol{\alpha} \\ &\approx \rho(\boldsymbol{\beta})\,\frac{\mathrm{e}^{\mathrm{i}\,\rho(\boldsymbol{\beta})\,k\,z}}{\mathrm{i}\,\lambda\,z}\,\mathrm{e}^{\frac{\mathrm{i}\,\pi\,\rho(\boldsymbol{\beta})}{\lambda\,z}\,\left\|\boldsymbol{x}-\frac{\lambda\,z}{\rho(\boldsymbol{\beta})}\,\boldsymbol{\beta}\right\|^2}, \end{aligned} \tag{219}$$

where Eq. (56) has been used to simplify the integral. Again, note that for $\boldsymbol{\beta}=\boldsymbol{0}$, the usual paraxial approximation is retrieved, see Eq. (58). Using this kernel, and introducing $\boldsymbol{s}=\lambda\,z\,\boldsymbol{\beta}/\rho(\boldsymbol{\beta})$ to simply the expressions, the propagation of the field writes:

$$\begin{aligned} a_z(\boldsymbol{x};\boldsymbol{\beta}) &= \iint a_0(\boldsymbol{x}')\,h_z(\boldsymbol{x}-\boldsymbol{x}';\boldsymbol{\beta})\,\mathrm{d}\boldsymbol{x}' \\ &\approx \rho(\boldsymbol{\beta})\,\frac{\mathrm{e}^{\mathrm{i}\,\rho(\boldsymbol{\beta})\,k\,z}}{\mathrm{i}\,\lambda\,z}\iint a_0(\boldsymbol{x}')\,\mathrm{e}^{\frac{\mathrm{i}\,\pi\,\rho(\boldsymbol{\beta})}{\lambda\,z}\,\left\|\boldsymbol{x}-\boldsymbol{x}'-\boldsymbol{s}\right\|^2}\,\mathrm{d}\boldsymbol{x}' \\ &\approx \rho(\boldsymbol{\beta})\,\frac{\mathrm{e}^{\mathrm{i}\,\rho(\boldsymbol{\beta})\,k\,z}}{\mathrm{i}\,\lambda\,z}\,\mathrm{e}^{\frac{\mathrm{i}\,\pi\,\rho(\boldsymbol{\beta})}{\lambda\,z}\,\|\boldsymbol{x}-\boldsymbol{s}\|^2} \\ &\quad\times\iint\left[a_0(\boldsymbol{x}')\,\mathrm{e}^{\frac{\mathrm{i}\,\pi\,\rho(\boldsymbol{\beta})}{\lambda\,z}\,\|\boldsymbol{x}'\|^2}\right]\mathrm{e}^{\frac{-\mathrm{i}\,2\,\pi\,\rho(\boldsymbol{\beta})}{\lambda\,z}\,(\boldsymbol{x}-\boldsymbol{s})^\top\cdot\boldsymbol{x}'}\,\mathrm{d}\boldsymbol{x}', \end{aligned} \tag{220}$$

which is readily a fumction of $\boldsymbol{x}-\boldsymbol{s}$ and where the integral amount to compute the 2-dimensional Fourier transform of the term in square brackets which is the auxiliary field $a_0(\boldsymbol{x})$ times a quadratic phasor.

Equations. (207) and (220) suggest to write the propagated field as:

$$u_z(\boldsymbol{x}) \approx a_z(\boldsymbol{x}-\boldsymbol{s})\,\mathrm{e}^{\mathrm{i}\,2\,\pi\,\boldsymbol{\beta}^\top\cdot\boldsymbol{x}}, \tag{221}$$

with $\boldsymbol{s}=\lambda\,z\,\boldsymbol{\beta}/\rho(\boldsymbol{\beta})$ and:

$$\begin{aligned} a_z(\boldsymbol{x}) &= \rho(\boldsymbol{\beta})\,\frac{\mathrm{e}^{\mathrm{i}\,\rho(\boldsymbol{\beta})\,k\,z}}{\mathrm{i}\,\lambda\,z}\,\mathrm{e}^{\frac{\mathrm{i}\,\pi\,\rho(\boldsymbol{\beta})}{\lambda\,z}\,\|\boldsymbol{x}\|^2} \\ &\quad\times\iint\left[a_0(\boldsymbol{x}')\,\mathrm{e}^{\frac{\mathrm{i}\,\pi\,\rho(\boldsymbol{\beta})}{\lambda\,z}\,\|\boldsymbol{x}'\|^2}\right]\mathrm{e}^{\frac{-\mathrm{i}\,2\,\pi\,\rho(\boldsymbol{\beta})}{\lambda\,z}\,\boldsymbol{x}^\top\cdot\boldsymbol{x}'}\,\mathrm{d}\boldsymbol{x}'. \end{aligned} \tag{222}$$

These equations implement a *tilted paraxial approximation* of the planar propagation. The tilted wavefront with respect to the auxiliary field is exactly preserved and induces (as expected) a shift of the field by $\boldsymbol{s}$. Hence, this tilted paraxial approximation can help achieving a better precision when the beam is tilted or when considering off-centered windows, notably if the same strategy as the 2-step Fresnel transform is exploited. Important for numerical computations: the approximation is separable in the two axes of the transverse plane.

See work of Matsushima et al. (2003)?

C The discrete Fourier transform

C.1 Uni-dimensional case

The Fourier transform of $f(x)$ at frequency α is defined by:

$$\widetilde{f}(\alpha) = \int_{-\infty}^{+\infty} f(x)\, \mathrm{e}^{-\mathrm{i}\, 2\, \pi\, \alpha\, x}\, \mathrm{d}x. \tag{223}$$

The inverse transform is given by:

$$f(x) = \int_{-\infty}^{+\infty} \widetilde{f}(\alpha)\, \mathrm{e}^{+\mathrm{i}\, 2\, \pi\, \alpha\, x}\, \mathrm{d}\alpha. \tag{224}$$

Using N evenly spaced positions $x_j = x_0 + j\, \delta x$ with δx the sampling step and for $j \in \{0, 1, ..., N-1\}$, $\widetilde{f}(\alpha)$ can be approximated by a Riemann sum:

$$\widetilde{f}(\alpha) \approx \sum_{j=0}^{N-1} f(x_j)\, \mathrm{e}^{-\mathrm{i}\, 2\, \pi\, \alpha\, x_j}\, |\delta x|. \tag{225}$$

To have an invertible discrete transform, the frequencies α must also be sampled with N samples. Considering a uniform sampling of the frequencies, the discrete frequencies are given by $\alpha_k = \alpha_0 + k\, \delta\alpha$ with $\delta\alpha$ the frequency sampling step and for $k \in \{0, 1, ..., N-1\}$. The sampled spectrum is then given by:

$$\widetilde{f}(\alpha_k) \approx |\delta x| \sum_{j=0}^{N-1} \mathrm{e}^{-\mathrm{i}\, 2\, \pi\, \alpha_k\, x_j}\, f(x_j) = |\delta x| \sum_{j=0}^{N-1} F_{k,j}\, f(x_j), \tag{226}$$

with:

$$F_{k,j} = \mathrm{e}^{-\mathrm{i}\, 2\, \pi\, \alpha_k\, x_j}. \tag{227}$$

Hence $|\delta x|\, \mathbf{F}$ is a linear operator implementing a discrete approximation of the continuous Fourier transform.

Following the same reasoning to approximate the inverse Fourier transform of $\widetilde{f}(\alpha)$ which yields $f(x)$, the inverse discrete Fourier transform should be implemented by $|\delta\alpha|\, \mathbf{F}^\star$ with $\mathbf{F}^\star$ the adjoint, that is the conjugate transpose, of $\mathbf{F}$ and $\delta\alpha$ the frequency sampling step. For $|\delta\alpha|\, \mathbf{F}^\star$ to really be the inverse of $|\delta x|\, \mathbf{F}$, the following conditions must hold:

$$|\delta x\, \delta\alpha|\, \left(\mathbf{F}^\star \cdot \mathbf{F}\right)_{j,k} = \begin{cases} 1 & \text{if } j = k, \\ 0 & \text{else.} \end{cases} \tag{228}$$

Expanding the left-hand side of this equation yields:

$$\begin{aligned}
|\delta x\,\delta\alpha|\left(\mathbf{F}^\star\cdot\mathbf{F}\right)_{j,k} &= |\delta x\,\delta\alpha|\sum_{\ell=0}^{N-1} F^\star_{j,\ell}\,F_{\ell,k}\\
&= |\delta x\,\delta\alpha|\sum_{\ell=0}^{N-1} \mathrm{e}^{\mathrm{i}\,2\,\pi\,\alpha_\ell\,(x_j-x_k)}\\
&= |\delta x\,\delta\alpha|\,\mathrm{e}^{\mathrm{i}\,2\,\pi\,\alpha_0\,(j-k)\,\delta x}\sum_{\ell=0}^{N-1} \mathrm{e}^{\mathrm{i}\,2\,\pi\,\delta\alpha\,\delta x\,(j-k)\,\ell}\\
&= |\delta x\,\delta\alpha|\,\mathrm{e}^{\mathrm{i}\,2\,\pi\,\alpha_0\,(j-k)\,\delta x}\begin{cases} N & \text{if } \psi = 1\\ \frac{1-\psi^N}{1-\psi} & \text{else}\end{cases}
\end{aligned} \tag{229}$$

We first assume that $j = k$, then all complex exponential terms in the right-hand side of Eq. (229) are equal to 1 and thus the first condition in Eq. (228) amounts to $N\,|\delta x\,\delta\alpha| = 1$. Using this result and assuming now that $j \neq k$, the second condition in Eq. (228) imposes that the sum in the right-hand side of Eq. (229) be equal to 0:

$$0 = \sum_{\ell=0}^{N-1} \mathrm{e}^{\mathrm{i}\,2\,\pi\,(j-k)\,\ell/N} = \sum_{\ell=0}^{N-1} \psi^\ell = \begin{cases} N & \text{if } \psi = 1\\ \frac{1-\psi^N}{1-\psi} & \text{else}\end{cases} \tag{230}$$

with $\psi = \mathrm{e}^{\pm\mathrm{i}\,2\,\pi\,(j-k)/N}$ and where $\pm$ is the sign of $\delta x\,\delta\alpha$. When $j \neq k$, $0 < |j-k| < N$ holds, it follows that $\psi \neq 1$ and thus that the above sum is equal to $(1-\psi^N)/(1-\psi)$. Now, since $j-k$ is integer, $\psi^N = 1$ whatever the values of j and k and the sum is thus equal to 0 as required.

To summarize, it is sufficient that the sampling condition $N\,|\delta x\,\delta\alpha| = 1$ holds to have $|\delta x|\,\mathbf{F}$ and $|\delta\alpha|\,\mathbf{F}^\star$ implement discrete approximation of the continuous Fourier transform and of its inverse. However, in order to have the signs in the complex exponents of the entries of $\mathbf{F}$ be the same as in the continuous version (as in Eq. (232) below), the sampling steps must have the same signs and the sampling condition writes:

$$N\,\delta x\,\delta\alpha = 1. \tag{231}$$

The coefficients of $\mathbf{F}$ are then given by:

$$F_{j,k} = \mathrm{e}^{-\mathrm{i}\,2\,\pi\,j\,k/N}. \tag{232}$$

Due to the sampling condition, the magnitude of the highest sampled frequency, the so-called **Nyquist frequency**, is (for an even number N of samples):

$$\alpha_{\max} = \frac{N}{2}\,|\delta\alpha| = \frac{1}{2\,|\delta x|} \tag{233}$$

as stated by Whittaker-Shannon theorem. In implementations of the discrete Fourier transform (DFT), it is usually assumed that the first sample is at the origin in the direct and in the conjugate spaces, hence:

$$\begin{aligned} x_0 &= 0\\ \alpha_0 &= 0\end{aligned} \tag{234}$$

by convention, not by necessity.

C.2 Multi-dimensional case

The results found for the uni-dimensional DFT can be generalized to d-dimensional DFT as follows.

The direct space is sampled on a $N_1 \times N_2 \times \ldots \times N_d$ Cartesian grid with sampling steps δx_1, δx_2, ..., and δx_d along the axes. The sampling condition given in Eq. (231) for the frequency step applies separately along each dimension $i \in \{1, 2, \ldots, d\}$:

$$N_i \, \delta x_i \, \delta \alpha_i = 1. \tag{235}$$

Using d-dimensional Cartesian indices $\boldsymbol{j} = (j_1, j_2, \ldots, j_d)$ and $\boldsymbol{k} = (k_1, k_2, \ldots, j_d)$, the coefficients of the direct DFT operator are given by:

$$F_{\boldsymbol{k},\boldsymbol{j}} = \mathrm{e}^{-\mathrm{i}\, 2\, \pi \, \langle\!\langle \boldsymbol{j}, \boldsymbol{k} \rangle\!\rangle} \tag{236}$$

with:

$$\langle\!\langle \boldsymbol{j}, \boldsymbol{k} \rangle\!\rangle = \sum_{i=1}^{d} \frac{j_i \, k_i}{N_i} \tag{237}$$

and the inverse of the DFT operator $\mathbf{F}$ is:

$$\mathbf{F}^{-1} = \frac{1}{\prod_{i=1}^{d} N_i} \, \mathbf{F}^{\star} \tag{238}$$

where $\mathbf{F}^{\star}$ is the adjoint, that is the conjugate transpose, of $\mathbf{F}$.

Equipped with this estimator, the continuous d-dimensional Fourier transform and its inverse may be approximated by:

$$\mathbb{F} = \left(\prod_{i=1}^{d} |\delta x_i| \right) \mathbf{F}, \tag{239}$$

$$\mathbb{F}^{-1} = \left(\prod_{i=1}^{d} |\delta \alpha_i| \right) \mathbf{F}^{\star} = \frac{1}{\prod_{i=1}^{d} N_i \, |\delta x_i|} \, \mathbf{F}^{\star}, \tag{240}$$

References

Max Born, Emil Wolf, A. B. Bhatia, P. C. Clemmow, D. Gabor, A. R. Stokes, A. M. Taylor, P. A. Wayman, and W. L. Wilcock. *Principles of Optics: Electromagnetic Theory of Propagation, Interference and Diffraction of Light*. Cambridge University Press, 7th edition, October 2002. ISBN 9781139644181. doi: 10.1017/cbo9781139644181.

J. W. Goodman. *Introduction to Fourier Optics*. Mc Graw-Hill, 2nd edition, 1996.

Sander Konijnenberg, Aurèle J.L. Adam, and H. Paul Urbach. *BSc Optics*. TU Delft Open, 2nd edition, 2022. ISBN 978-94-6366-396-0. doi: 10.5074/t.2021.003. URL https://textbooks.open.tudelft.nl/textbooks/catalog/book/42.

Christophe Kopp and Patrick Meyrueis. Near-field fresnel diffraction: improvement of a numerical propagator. *Optics Communications*, 158(1–6):7–10, December 1998. ISSN 0030-4018. doi: 10.1016/s0030-4018(98)00549-5.

Éamon Lalor. Conditions for the validity of the angular spectrum of plane waves*. *Journal of the Optical Society of America*, 58(9):1235, September 1968. ISSN 0030-3941. doi: 10.1364/josa.58.001235.

David Mas, Javier Garcia, Carlos Ferreira, Luis M. Bernardo, and Francisco Marinho. Fast algorithms for free-space diffraction patterns calculation. *Optics Communications*, 164(4-6):233–245, jun 1999. doi: 10.1016/s0030-4018(99)00201-1.

Kyoji Matsushima, Hagen Schimmel, and Frank Wyrowski. Fast calculation method for optical diffraction on tilted planes by use of the angular spectrum of plane waves. *Journal of the Optical Society of America A*, 20(9):1755, September 2003. ISSN 1520-8532. doi: 10.1364/josaa.20.001755.

Lord Rayleigh. On the passage of waves through apertures in plane screens, and allied problems. *The London, Edinburgh, and Dublin Philosophical Magazine and Journal of Science*, 43(263):259–272, April 1897. ISSN 1941-5990. doi: 10.1080/14786449708620990.

P. H. Roberts. A wave optics propagation code. techreport TR-760, the Optical Sciences Company, Anaheim, Calif., 1986.

Jason D. Schmidt. *Numerical Simulation of Optical Wave Propagation*. SPIE, 2010. ISBN 978-0-8194-8326-3.

Arnold Sommerfeld. Mathematische Theorie der Diffraction: Mit einer Tafel. *Math. Ann.*, 47:317–374, 1896.

W. H. Southwell. Validity of the fresnel approximation in the near field. *Journal of the Optical Society of America*, 71(1):7, January 1981. ISSN 0030-3941. doi: 10.1364/josa.71.000007.

Edward A. Sziklas and A. E. Siegman. Diffraction calculations using fast fourier transform methods. *Proceedings of the IEEE*, 62(3):410–412, 1974. ISSN 0018-9219. doi: 10.1109/proc.1974.9438.

Edward A. Sziklas and A. E. Siegman. Mode calculations in unstable resonators with flowing saturable gain 2: Fast fourier transform method. *Applied Optics*, 14(8):1874, August 1975. ISSN 1539-4522. doi: 10.1364/ao.14.001874.

G. A. Tyler and D. L. Fried. A wave optics propagation algorithm. techreport TR-451, the Optical Sciences Company, Anaheim, Calif., 1982.